CHALMERS

A Rapid Acquisition GPS receiver based on ultra tightly coupled IMU and GPS

Master's Thesis in Communication Engineering

GABRIEL GARCIA

Department of Earth and Space Sciences
CHALMERS UNIVERSITY OF TECHNOLOGY
Göteborg, Sweden 2010
Master's Thesis 2010:08

MASTER'S THESIS 2010:08

A Rapid Acquisition GPS receiver based on ultra tightly coupled IMU and GPS

Master's Thesis in Communication Engineering

GABRIEL GARCIA

Department of Earth and Space Sciences
CHALMERS UNIVERSITY OF TECHNOLOGY
Göteborg, Sweden 2010

A Rapid Acquisition GPS receiver based on ultra tightly coupled IMU and GPS

GABRIEL GARCIA

©GABRIEL GARCIA, 2010

Master's Thesis 2010:08
ISSN tbd
Department of Earth and Space Sciences
Chalmers University of Technology
SE-412 96 Göteborg
Sweden
Telephone: + 46 (0)31-772 1000

Chalmers Reproservice
Göteborg, Sweden 2010

A Rapid Acquisition GPS receiver based on ultra tightly coupled IMU and GPS

Master's Thesis in Communication Engineering
GABRIEL GARCIA
Department of Earth and Space Sciences
Chalmers University of Technology

Abstract

Nowadays, the importance to obtain position in weak signal environments, such as indoors, has increased in order to take a step forward in the greater use of GPS. However, the weak signal environment may include several negative factors such as low signal to noise ratio, signal jamming and interference among others that shall be studied. The present thesis work proposes an open loop approach to deal with the signal dynamics. A Doppler model is proposed in order to remove the dynamics of the incoming GPS signal with the aid of an Inertial Measurement Unit (IMU). The model is broken down into calculating the satellite dynamics, the receiver dynamics and the receiver's oscillator dynamics. An error budget is created in order to see the unpredictable errors and their influence. A bandwidth analysis is also performed in order to analyze the effects of the dynamics in the receiver's phase locked loop (PLL), more specifically in the loop bandwidth. Available measurements from a high tech IMU and a GPS receiver oscillator are analyzed to quantify the time dependant errors.

An algorithm to account for the satellite dynamics is proposed with an accuracy Doppler error of $\pm.0005$ Hz. It is shown that the errors from the IMU are dominant in the error budget. However, the receiver dynamics errors are reduced: For a scenario where a vehicle enters a tunnel at 100 km/h and 50 seconds later exits the tunnel with a speed of 28 km/h it is shown that the dynamics of the signal can be reduced from 100 Hz to 6 Hz after implementing the open loop approach. The errors introduced by the oscillator are also shown to be significant with up to 2.58 Hz for L1 GPS signal.

These conclusions give arise to the use of lower bandwidth usage in the PLL. Higher signal to noise ratio can be deduced and rapid acquisition and reacquisition of the signal is possible, meaning the GPS signal can be tracked immediately after blockage situations.

Keywords: GPS, INS, Receiver, Integration, Dynamics, Satellite, Oscillator, Doppler Effect, Doppler Model, Inertial sensors, Accelerometer, Gyroscope

Contents

Aknowledgements

I am grateful with all the people that I have had the opportunity to work during this thesis work. They support from the initial to the final stages enabled me to develop an understanding on the subject, especially:

Erik Steinmetz (supervisor), To whom I owe my deepest gratitude for his time; involving interesting discussions, guidance and ideas along the thesis work. For his help with the data processing and his patience and understanding along the project.

Ragne Emardson (supervisor), who made available his support in an important number of ways such as discussions, guidance, ideas and feedback throughout the project.

Per Jarlemark(supervisor), for his help with the measurements understanding, discussions and ideas during the thesis work.

Jan Johansson (examiner), for the useful comments and help with my report and work as well for introducing me to the GPS world.

I would also like to thank my friends, who always encouraged me through hard times.

Last but not least, I would like to thank my family and their indescribable support through all this time, for giving me the necessary strength and courage to pursue my projects and goals.

Göteborg May 2010
Gabriel Garcia

1 Introduction

This master thesis is intended to perform a feasibility study on the design of a rapid acquisition Global Positioning System (GPS) receiver based on ultra tightly coupled Inertial Measurement Unit (IMU) and Global Position System (GPS) strategies.

1.1 Background

During the last years the use of Global Navigation Satellite Systems (GNSS), more specifically Global Positioning System (GPS), for positioning and navigation have been globally widespread. Nowadays, the importance to obtain position in weak signal environments, such as indoors, has increased in order to take a step forward in the greater use of GPS. The weak signal environment may include several negative factors such as low signal to noise ratio, signal jamming and interference among others.

One of the possible approaches to overcome the weak signals scenario is the coupling of an Inertial Measurement Unit (IMU) along with the GPS receiver. These IMU-aided GPS receivers are usually referred to as coupled IMU/GPS receivers. The IMU provides aid to the GPS phase/frequency and code tracking loops. By calculating the velocity information from acceleration data, Doppler information can be extracted and then used to remove the high dynamics of the received signal to improve the tracking in weak signal scenarios.

1.2 Purpose

The purpose of this project is to make a feasibility study on the implementation of an open loop tracking approach using ultra-tight GPS/IMU strategies. Furthermore, the thesis will produce a design of a rapid acquisition receiver IMU-supported GPS receiver with improved tracking in low signal conditions.

The open loop tracking approach involves the design of a Doppler model that considers all the essential players in the high dynamics scenario that give a arise to a change in frequency on the received signal. This model will then give us the necessary tools to improve the signal tracking and calculate an error budget in order to perform the feasibility study.

The receiver will be an important contribution to the field of indoor navigation and hostile environment conditions and the mentioned error acquaintances will give some perspective in order to realize improvement for future work.

2 Theory

2.1 Global Positioning System

2.1.1 Overview

Global Positioning System (GPS) is a satellite-based radio-navigation system. The system was developed by the U.S. Department of defense under its NAVSTAR satellite program (Grewal, 2001). GPS consists of 3 different segments: the space segment, the control segment and the user segment.

Space Segment The space segment as its name implies involves all the aspects concerning the GPS satellites. GPS has 24 (32 satellites are now in orbit) distributed in 6 equally spaced circular orbital planes with an inclination of 55 ° (relative to the equator) and an

approximate radio of 22,200 kilometers. The satellites have an orbital period of around 11 hours and 58 minutes. It is important to mention that the orbits are not geosynchronous leading to a change in geometric view from the end-user's perspective; these geometric changes have impact on the position accuracy calculation, however, they are predictable. The main reason for this GPS constellation design is to assure that the end-user, located anywhere on the globe, will have a line of sight with at least 4 GPS satellites at the same time at anytime (Farrel and Barth, 1999).

Control Segment The control's segment main purpose is to check the status of the space segment. This segment includes: 1 master control, 6 monitor stations and 4 ground antennas spread all over the globe. The master control station, located at Colorado Springs collects the tracking data of the monitoring stations and calculates the satellite's orbit and clock parameters using a Kalman estimator. Then, these estimations are sent to the control ground stations that have the task of uploading the data to the satellites (Hofmann-Wellenhoff, 2001).

User Segment The user segment consists basically in the GPS users that own a GPS receiver with its antenna. Inside the user segment there are two important categories: military use and the civilian use. The equipment receives the signals from the satellites in order to provide positioning, velocity and precise timing information (Hofmann-Wellenhoff, 2001).

2.1.2 Signals

GPS is a passive system; thereby the availability of the system is intended for an unlimited number of users. All satellite transmissions are derived from the fundamental frequency $f_o = 10.23$ MHz that is available from the set of on-board atomic clocks. Each GPS satellite transmits on two L-band frequencies by using Code Division Multiple Access (CDMA). When multiplying the fundamental frequency times 154 we obtain 1575.42 MHz, which is denoted as the L1 carrier; multiplying the same fundamental frequency times 120 gives arise to L2 carrier at 1227.60 MHz (Leick, 1990).

Three pseudorandom noise (PRN) codes are embedded with each satellite. All codes are bi-phased modulated on the carrier frequencies L1 and L2, this is known as spread spectrum and it is used to make the signal more resistant to jamming and interference and sometimes to limit the power flux density(Farrel and Barth, 1999).

The Course/Acquisition (C/A) code modulates the L1 carrier phase. It has a length of 1023 chips, a rate of 1.023 MHz and a period of 1 ms. There exists a different C/A PRN code for each satellite that is nearly orthogonal to each of the other C/A PRN codes belonging to the other satellites. Although the satellites transmit at the same two frequencies (L1 and L2) the GPS receiver is able to recognize the satellite by correlating an internally generated version of the C/A PRN with the received signal(Farrel and Barth, 1999).

The precise code (P) modulates both L1 and L2 carrier phases. It has a rate of 10.23 MHz and a period of 7 days. The last code is the so-called Y code. This Y-code is only available on the antispoofing (AS) mode of operation. It is an encrypted version of the P-code and it requires a classified AS module in the receiver, therefore it is only available to authorized users with cryptographic keys (Farrel and Barth, 1999).

Each satellite also transmits a navigation message, which also modulates the L1 C/A code signal. The navigation message is a 50 bit/s signal that consists on information about the satellite's orbit, health and clock correction among other parameters. The whole

navigation message frame is divided into 5 subframes. It takes 6 seconds to transmit each one of them. The first subframe contains polynomial coefficients to correct the on-board satellite time to GPS time. The second and the third subframes consist on the ephemeris of the broadcasting satellite. The ephemerides are precise orbital information. The fourth subframe is mainly for special messages such as ionospheric correction terms and coefficients for GPS to UTC time conversion. The fifth subframe contains the ephemeris and health status for one of the 25 (now 32) satellites. This subframe is subcommutated 25 times in order to receive all the ephemeris from the whole GPS constellation satellites, therefore it takes 12.5 minutes to get the complete orbital information, which is known as almanac (Grewal, 2001).

2.1.3 Observables

In order to find the three dimensional position of the user a so-called range should be determined from the user to at least 4 satellites with known positions in space. This range can be defined as the distance from the user to each of the satellites. Having these ranges, then a point can be solved mathematically, where these set of ranges take place. The ranges can be obtained either from measured time or phase differences and are denoted as observables Grewal (2001).

However, the ranges are measured by comparing the received signal and the internal replica generated in the receiver. The received signal is generated by the satellite clocks, while the replica is generated using the own receiver's clock. This means that there exist unavoidable timing errors that will cause the geometric distance to differ from the true distance value; therefore, the error-influenced ranges are called pseudoranges. Other factors will also introduce errors in the pseudoranges, such as the troposphere and ionosphere; this will be discussed later on the thesis work. Meanwhile the simplified pseudoranges' equations for the code and phase cases only containing the clock errors can be seen in 2.1 and 2.2 , respectively (Hofmann-Wellenhoff, 2001):

$$R = \rho + c\Delta\delta t \tag{2.1}$$

$$\Phi = \frac{1}{\lambda}\rho + \frac{c}{\lambda}\Delta\delta t - N \tag{2.2}$$

For the code phase, expressed in meters, R is the code pseudorange, ρ is the true distance and $c\Delta\delta t$ is the combined clock errors (satellite and receiver). For the phase case, expressed in cycles, Φ is the measurable fractional phase and N symbolizes an integer ambiguity parameter, in other words, the unknown number of integer cycles at the initial epoch; these parameters need to be solved prior to calculating the receiver's position.

If clock errors did not exist, the position of the receiver could be solved only using 3 satellites. However, due to the clock errors at least four satellites are needed.

2.1.4 Error Sources

The pseudoranges (code and phase) are not only affected by clock errors. They are also affected by other types of errors. Generally, the errors can be divided into three groups: satellite related errors, propagation errors and receiver errors, see Table 2.1.

First we have the satellite related errors, the satellite clock and orbital errors. The satellite clock, over time, will drift away from the GPS system time. This error can be compensated by using the clock correction parameters sent in the broadcast ephemeris. The orbital errors can be defined as the errors in the predicted orbital parameters sent in the broadcast ephemeris. The three components of ephemeris error are the radial, tangent,

Source	Effect
Satellite	Clock bias Orbital Errors
Signal Propagation	Ionospheric refraction Tropospheric refraction
Receiver	Antenna phase center variation Clock bias Multipath

Table 2.1: Error Sources and Effects (Hofmann-Wellenhoff, 2001)

and cross track components where the radial component is the one affecting the ranging accuracy and turns out to be around 1 meter. To mitigate this error, post-processed precise ephemeris can be used reducing the radial error even up to .05 meters. Another solution is to differentiate between two receivers (when available); this solution will eliminate the satellite biases (Farrel and Barth, 1999).

Second we have the signal propagation errors. These errors can be classified into two categories: dispersive and nondispersive. The nondispersive portion is related to the troposphere (although some other atmospheric portions are not considered) and the dispersive portion is related to the ionosphere. The troposphere, located from 8 to 40 km above the Earth's surface, suffers from constant changes in temperature, pressure and humidity. These changes affect the refractive index of the medium, causing a so called tropospheric delay, resulting in errors on the measured range at the receiver. The tropospheric delay errors are consistent among the L1, L2, and carrier and code signals since the delay does not depend on frequency. The delay is commonly represented as having a dry and a wet component, accounting for 90 % and 10 % of the tropospheric delay, respectively. The wet component is difficult to model due to the variations and the dependence on the water vapor content on the troposphere. However, there are different models in order to compensate for this component. On the other hand, the dry component also known as hydrostatic delay is relatively easy to model (Farrel and Barth, 1999). The dispersive portion of the propagation errors is related to the ionosphere, located 50 km above the Earth's surface and consisting on ionized air. Changes in the level of ionization affect the refractive index, therefore affecting the traveling time of the signal. The ionospheric delay is frequency dependant and is proportional to $\frac{1}{f^2}$, where f is the signal frequency. Due to this dispersive effect, the ionospheric delay can be eliminated by using two signals with different frequencies, in this case L1 and L2. A simple linear combination between these signals can account for the errors derived from the ionosphere. In the case of short baseline relative positioning availability, having two close receivers experiencing from the same weather and propagation effects, differentiation methods to mitigate the propagation errors can be implemented (Farrel and Barth, 1999).

Finally we have the receiver related errors: the receiver clock, the antenna phase center and the multipath errors. The receiver clock bias can be handled with different methods. One option is to use differencing strategies between two satellites. Another option is to develop a dynamic model to estimate the change in the clock error using Kalman filtering. And the third and more common consists on solving for the receiver clock error together with the receiver coordinates (4 satellites are needed as stated in the observables section). The antenna phase center variations depend highly in the used antenna; functions depending on the type of antenna, azimuth and elevation angles have been developed as well as laboratory tests in order to model this effect. Multipath effect is caused by reflecting surfaces near the receiver causing signals to arrive via more than one path. There is no

general model for this effect, however, multipath reduction can be achieved by selecting the correct antenna and using the antenna in places with few reflection surfaces; improved receiver technology and signal and data processing are also common solutions. It is important to mention that multipath is frequency dependant, therefore, it affects more to code ranges rather than carrier phases (Hofmann-Wellenhoff, 2001).

Besides the already mentioned error sources, some random noise should be added to the pseudoranges. This random noise contains observation noise plus some random multipath effects. The random noise effect on the pseudoranges is depicted in Table 2.2(Hofmann-Wellenhoff, 2001).

Pseudorange	**Noise**
C/A code range	10-300 cm
P code range	10-30 cm
Phase range	0.2-5 mm

Table 2.2: Pseudoranges' random noise

2.1.5 Signal Acquisition and Tracking

Before providing a navigation solution in the GPS receiver, a sequence of operations must be performed by the receiver in order to access the GPS signal. This sequence is enumerated as follows(Grewal, 2001):

1. Determine visible satellites to the antenna
2. Determine approximate Doppler of each visible satellite
3. Signal search in frequency and C/A code phase
4. Lock and track C/A code
5. Lock and track carrier
6. Data bit synchronization and navigation message demodulation

Determine visible satellites It is always a priority to minimize the time between the receiver turn-on and the navigation solution. This time is defined as the time to first fix (TTFF). Therefore, the receiver should focus on the satellite signals available above the horizon. The receiver can perform a search on the visible satellites when knowing their approximate location and time either with the almanac saved during last operations or manually entered satellite positions by the user on the receiver (Grewal, 2001).

Signal Doppler estimation If the Doppler shifts from the visible satellites are known the TTFF can be further reduced. This Doppler shift can be used to perform a more efficient frequency search of the signals. The Doppler shift can be calculated knowing the approximate position, time and valid almanac data from the satellites (Grewal, 2001).

Signal search in frequency and C/A code phase The C/A code search is necessary since GPS signals are spread-spectrum signals, where the C/A code spreads the signal power over a wide bandwidth. The signal needs to be despread in order to raise the signal to noise ratio to a usable level. This is achieved using a replica code in the receiver aligned with the received code and correlating them. When the correlation energy is over a certain threshold, the signal is said to be lock and detected. The frequency search is necessary since GPS uses high carrier frequencies and the satellites experiment large velocities causing a doppler shift in the received signals (as much as $\pm$ 5 KHz). Moreover, the oscillator in the receiver will also cause a frequency uncertainty of several hertz. The frequency search starts from the estimated Doppler frequency and then alternately selects frequencies above and below the estimate until the frequency is detected (Grewal, 2001).

C/A code lock and tracking After detection, the code tracking loop is triggered, the tracking is necessary in order to maintain the receiver-generated code replica lined up with the incoming code as precisely as possible. It is common to use a Delay Locked Loop (DLL) in GPS receivers (Grewal, 2001).

Carrier lock and tracking The carrier phase tracking has different purposes. First, to have a phase reference for coherent detection of the GPS biphase modulated data. Another purpose is to provide velocity measurements (phase rate). Third, to obtain integrated Doppler in order to aid the code tracking loop. The last purpose is to obtain precise carrier phase pseudorange measurements. The carrier phase tracking is achieved by means of a Phase-Locked Loop (PLL) (Grewal, 2001).

Bit synchronization and navigation message demodulation When the PLL is locked to the GPS signal, bit synchronization is needed in order to locate the bit boundaries. The input stream is chopped into 20 ms long bins and then an evaluation using statistics is performed to locate where the bit values change sign. After the synchronization has been achieved, demodulation of the data bits can occur in order to extract the navigation message to find the navigation solution (Grewal, 2001).

2.1.6 Tracking Loop Architecture

Conventional GPS receivers use basically two types of tracking loops as we have discussed in the last section: code and carrier. The code loop despreads the incoming signal using the proper PRN code, leaving then the modulated data. Thereafter, the carrier-tracking loop demodulates the data bits.

A phase lock loop (PLL) is a control system that compares the phase of an input signal with a phase signal derived from its oscillator. The PLL adjusts then the frequency of the oscillator to keep the phases matched. It is an important part in the GPS receiver since the carrier tracking loop is essential. In this section an overview of the PLL functions is presented. A generic GPS carrier phase is shown in Figure 2.1 (Babu and Wang, 2005).

The GPS antenna at the receiver captures all the GPS signals coming from the visible satellites. The signals go through the radio frequency RF front end normally consisting on matching circuits, a low noise amplifier (LNA), coarse filters to reject unwanted signals and mixers circuitry for downconversion. The signals are sampled and downconverted to an intermediate frequency (IF), normally between 1 and 20 MHz for further processing. At this point all the GPS signals are superimposed one over another, therefore parallel channels shall be used to acquire and track each of the different satellite's signals. The frequency and carrier tracking is then performed by the individual PLLs (Chiou, 2005).

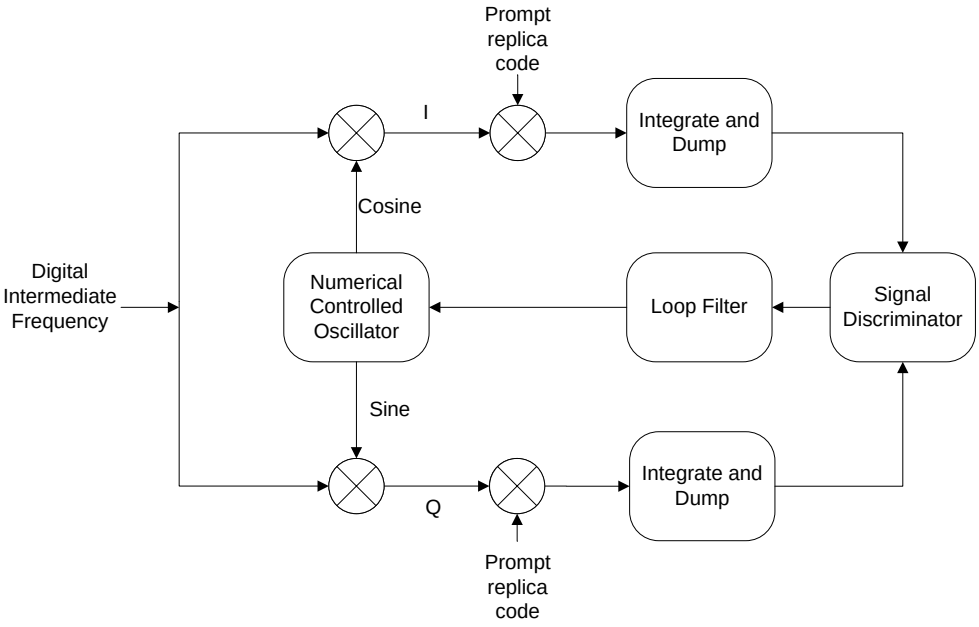

Figure 2.1: Generic Carrier Phase Tracking Loop

The next step is called carrier wipeoff operation. The purpose of this step is to downconvert the signal to the baseband. This is achieved by multiplying the carrier replica with the incoming digital IF signal. The frequency of the replica is obtained by measuring the phase and frequency offset due to the receiver and clock dynamics. A device called voltage controlled oscillator (VCO), numerical control oscillator (NCO) for mathematical purposes, is in charge of generating the replica. The upper branch is multiplied by the cosine carrier replica while the lower branch is multiplied by the sine. The result from the upper branch is called the in-phase channel (I) and the result from the lower branch is called the quadrature channel (Q). In order to finally take both the I and Q signals to the baseband they are multiplied by the code replica, that changes with every satellite(Chiou, 2005).

After the signal is downconverted to the baseband an operation called "integration and dump" takes place. The operation performs a measurement-averaging over one or more code periods in order to suppress noise. The longer the averaging time is, more noise is suppressed.

Thereafter, the signal goes through a phase discriminator. The discriminator measures the phase offset between the true received carrier and the replicated carrier. The output of this operation serves as control input to the loop filter.

The loop filter is a compensator designed to track the phase and frequency of the input carrier with the desired dynamic range and noise suppression performance. The Loop Filter's output is a frequency control command for the NCO which then steers the replicated carrier frequency to maintain the input carrier and the replica locked, in other words, to keep the phase error as close to zero as possible(Chiou, 2005). The bandwidth of the loop filter is one of the most important parameters when designing a PLL for a GPS receiver since the bandwidth is related to the ability of the receiver to track dynamics; this will be discussed in later sections.

2.2 Inertial Navigation

This section will give an overview of inertial navigation as well as its main sensors and errors. Inertial navigation can be defined as an autonomous navigation technique used

to track position and orientation of an object relative to a known starting point, orientation and velocity. The technique is based on the processing of measurements performed by the so-called inertial sensors: accelerometers and gyroscopes. Typically, an inertial measurement unit (IMU) contains three orthogonal gyroscopes as well as three orthogonal accelerometers. Gyroscopes have the task to measure angular velocity and accelerometers take care of the linear acceleration (Woodman, 2007).

The most important advantages of inertial navigation are (Grewal, 2001):

- It is an autonomous system, no external aids or visibility conditions (contrary with GPS) are needed. The system can operate indoors, underwater, outdoors.
- Suited for integrated navigation, guidance and control of the desired object.
- Immune to jamming since the system does not emit or receives detectable radiation.

The most important disadvantages are summed up (Grewal, 2001):

- Navigation errors increase with time due to the sensors' nature.
- Size and Cost. Early inertial navigation systems weighted tens of kilograms, therefore increasing the cost in acquisition, maintenance and operation. However, nowadays we can find systems weighing a few kilograms and more recently micro-machined electromechanical systems (MEMS) have been developed to shrink size and reduce weight considerably to only a few centimeters and grams, respectively.

Generally, IMUs are classified into two categories: stable platform systems and strapdown systems. The main difference relies in the frame of reference in which each of the systems' gyroscopes and accelerometers operate. The navigation system's frame of reference is denoted as body frame and the frame of reference where the navigation takes place is denoted as the global frame (Woodman, 2007). The frames' difference can be better explained observing Figure 2.2.

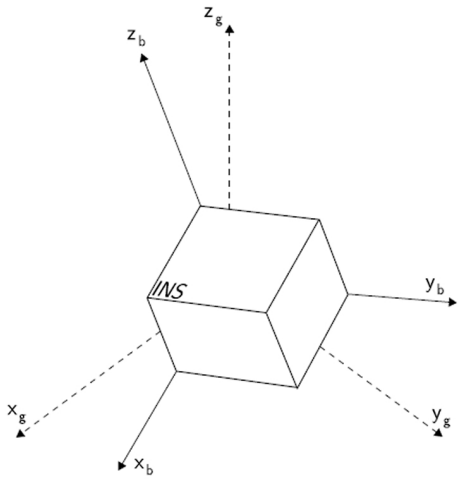

Figure 2.2: Global and body frames (Woodman, 2007)

2.2.1 Stable Platform Systems

In this type of system the inertial sensors are mounted on a rigid platform isolated from the rotations of the host object by a set of three or four gimbals as can be seen in Figure 2.3. The gimbals allow the platform freedom in the three axes; consequently, the measurements are quantified in the global frame. The gyroscopes measure any platform rotation, correction signals are sent then to torque motors to rotate the gimbals to cancel out the rotations. Orientation is then tracked by extracting the angles between adjacent gimbals. Position is calculated from the double integration of the accelerometer signals. The algorithm is depicted in Figure 2.4 (Woodman, 2007).

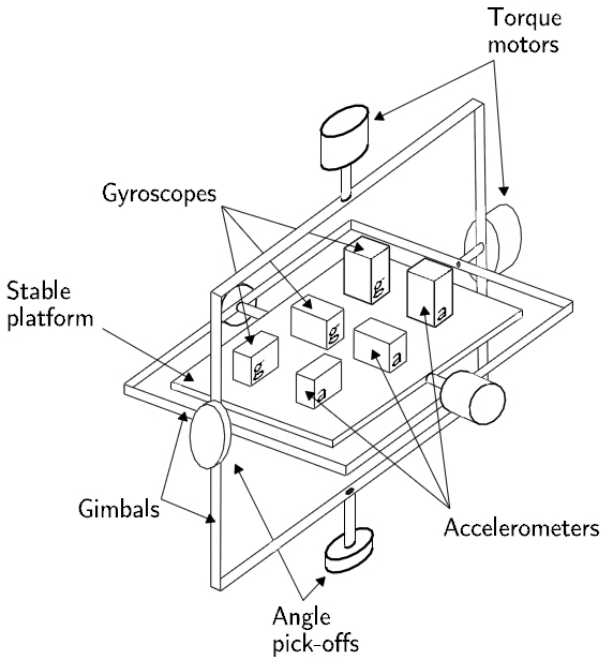

Figure 2.3: Stable platform IMU (Woodman, 2007)

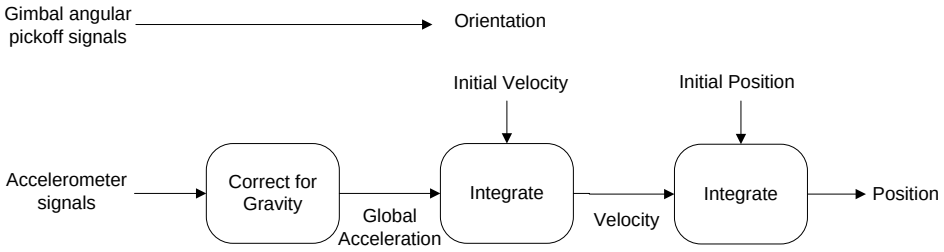

Figure 2.4: Stable platform inertial navigation algorithm (Woodman, 2007)

2.2.2 Strapdown Systems

In this kind of system the inertial sensors are hard mounted ("strapped down") onto the host object as can be observed in Figure 2.5, therefore, the measurements in this case are quantified in the body frame rather than the global frame. Orientation is calculated by integrating the signals from the rate gyroscopes. To keep track of the position, the accelerometer signals are mapped into the global frame using the previously calculated orientation and then the global acceleration is double integrated to end up with the position solution. The algorithm is shown in Figure 2.6. Nowadays, due to the system's mechanical

simplicity and physically smaller size than the stable platform systems, strapdown systems are more commonly used(Woodman, 2007).

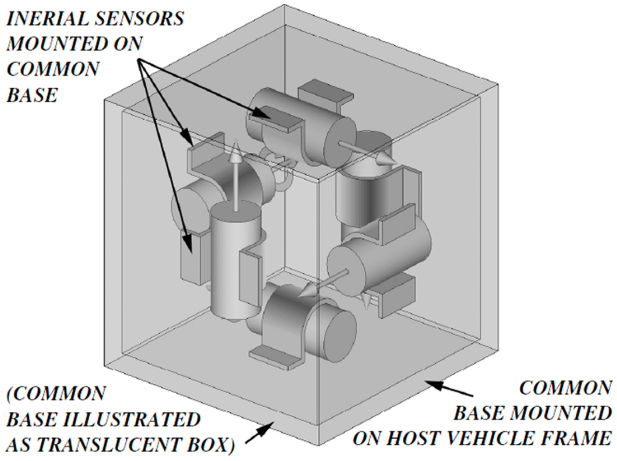

Figure 2.5: Strapdown IMU (Grewal, 2001)

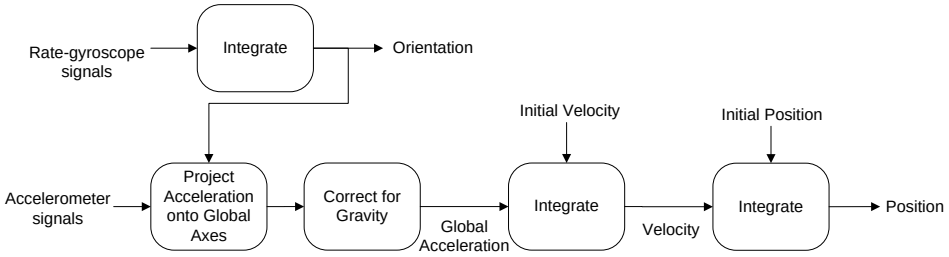

Figure 2.6: Strapdown inertial navigation algorithm (Woodman, 2007)

2.2.3 Gyroscopes

A gyroscope is a device used to measure orientation. It relies on the principles of angular momentum. Nowadays, different types of gyroscopes are in use. Among the main types we can find the mechanical gyroscopes, the optical gyroscopes and the micro-electrical mechanical system (MEMS) gyroscope.

A conventional mechanical gyroscope consists of a spinning wheel (rotor) mounted on two gimbals. This configuration allows the spinning wheel to rotate in 3 axes. The mechanical device is then subjected to any kind of rotation, due to the conservation of angular momentum the rotation of the wheel will remain at a constant global orientation changing the angles between the gimbals. These angles are then measured in order to track orientation.

The optical gyroscopes use the interference of light to measure angular velocity, not orientation as the mechanical type. It relies in the Sagna Effect. Two light beams are fired into a coil of optical fibre in opposite directions. When the coil is undergoing under rotation, the beam travelling in the direction of rotation will take longer to travel through the fiber to the other end. At the end of the coil the two light beams are summed up; due to the phase shift difference between the two light beams the intensity of the light will change depending on the angular velocity (Woodman, 2007).

MEMS gyroscopes are still under continue development. They are built up from silicon micro-machining sensors and they are cheap to manufacture. MEMS gyroscopes make use of the so called Coriolis Effect that states that in a frame of reference a mass m rotating at an angular velocity ω with a velocity v suffers from a force given by (Woodman, 2007):

$$F = -2m(\omega \times \upsilon) \tag{2.3}$$

The Coriolis Effect can be measured using vibrating element geometries. Even though MEMS sensors cannot achieve the same quality as the optical ones they have several advantages such as: small size, low weight, low power consumption and cold start up time, cheap to produce. Therefore, it is common to use MEMS gyroscopes in GPS/INS architectures(Woodman, 2007).

2.2.4 Error Characteristics

When using sensors such as gyroscopes, inherent errors arise in the measurements. These errors affect then the output signal, which in the case of the gyroscope is the measured orientation. Due to the characteristics of the IMU used in this thesis, this section will analyze the errors especially in MEMS gyroscopes.

Constant Bias This bias is the offset of the output from the true value, in other words the average output from the gyroscope when not suffering any kind of rotation. This constant bias ϵ will have an effect on the integrated orientation, causing an angular error given by:

$$\theta(t) = \epsilon \cdot t \tag{2.4}$$

The solution for this error is to take a long term average of the output on steady state (without rotation). Then this average is subtracted from the gyro's output to compensate for the error.

Angle Random Walk The output of the gyroscope will also be affected by a white noise sequence due to thermo-mechanical noise which fluctuates faster than the sampling rate of the sensor. This white noise sequence is simply a sequence of zero-mean uncorrelated random variables. Each variable is identically distributed and has a finite variance of σ^2. When this sequence is integrated the noise gives arise to a zero-mean random walk error with a standard deviation that goes proportionally with time, given by:

$$\sigma_\theta(t) = \sigma \cdot \sqrt{\delta t \cdot t} \tag{2.5}$$

It is typical to find the angle random walk specifications with units $degrees/\sqrt{Hz}$ (Woodman, 2007).

Bias Stability Bias stability or flicker noise is another important factor that will have a negative effect on the sensors' measurements. The bias of the gyroscope will be affected by flicker noise caused mainly by the electronics in the sensor. These fluctuations are typically modeled as random walk. A bias stability measurement describes how the bias will change over a determined period of time with certain conditions. The measurement is specified as a 1σ value with units degrees/hour. When integrating this flicker error, assuming a random walk model, the integrated output will be affected by a second order random walk in the orientation angle. It is important to mention that in reality flicker fluctuations do not behave as random walk. However this model works fine for short periods of time(Woodman, 2007).

Temperature effects Temperature also plays a significant role in the sensor errors. Temperature changes induced by environmental change or self sensor heating will cause a movement in the bias. This error will grow linearly with time just as with the constant bias. However, most of the IMUs contain internal temperature sensors that can be used to compensate for the induced bias effects due to temperature(Woodman, 2007).

Calibration errors The calibration errors include aspects such as scale factors, alignments and linearities of the gyros. These kinds of errors can be only observed when the gyro is turning, thus, causing additional drift in the integrated signal. It is possible to measure and compensate the calibration errors. There are some IMUs that include internal corrections for the calibration errors(Woodman, 2007).

2.2.5 Accelerometers

An accelerometer is a device that measures the physical acceleration experienced by an object relative to freefall. Accelerometers can be classified as either mechanical or solid state devices. A new type of accelerometers, micro-machined silicon accelerometers (MEMS) have been recently developed pursuing better quality measurements as well as small sized devices (Woodman, 2007).

A mechanical accelerometer basically consists on a mass suspended on springs. The displacement of the mass is measured whenever there is force acting on it. The result is signal proportional to the force F acting on the suspended mass in certain axis. In order to calculate the acceleration Newton's second law is applied:

$$F = ma \tag{2.6}$$

The solid state accelerometers can be subdivided into several groups like surface acoustic wave, vibratory, silicon, quartz devices, etc. Solid-state accelerometers are small and reliable(Woodman, 2007).

Recently, MEMS accelerometers have been in development. They rely in the same principles as the mechanic and solid state accelerometers. However, MEMS accelerometers are small, light and they have low power consumption as well as low cold start up times. Although they are not as accurate as the mechanical and solid state accelerometers, their performance is improving with time and they are perfectly suited for GPS/INS implementations.

2.2.6 Error Characteristics

Accelerometers have inherent errors just as the gyroscopes. These errors affect then the output signal, which in the case of the accelerometers is the final position. As expected, the errors are similar to the gyroscope ones. However, the errors in the accelerometers are double integrated, since normally they are used to calculate the position of the host object. For explanatory purposes the errors are explained having in mind the final position calculation.

Constant Bias The bias in this case is the offset of the accelerometer's output from the true value, this offset is given in m/s^2. This bias will have an effect on the calculated position given by:

$$\sigma(t) = \epsilon \cdot \frac{t^2}{2} \tag{2.7}$$

The same approach as in the gyroscopes in order to compensate for the error can be implemented. A long term average can be calculated and subtracted from the accelerometers' output when not suffering any acceleration. However, due to the gravity component precise orientation of the accelerometer shall be known(Woodman, 2007).

Thermo-mechanical white noise The output from the accelerometer is affected by a white noise sequence. As shown in the gyroscope error characteristics, when the error is integrated a random walk error is created. In this case after one integral a velocity random walk error is produced. When the double integration takes place to calculate the position the error creates a second order random walk error with zero mean and standard deviation given by(Woodman, 2007):

$$\sigma_s(t) = \sigma \cdot t^{3/2} \cdot \sqrt{\frac{\delta t}{3}} \tag{2.8}$$

Bias stability MEMS accelerometers also suffer from flicker noise. This noise is modeled as random walk noise as described in the gyroscope sections. When applying this same model flicker noise produces a second order random walk in velocity proportional to $t^{3/2}$ and a third order random walk in position proportional to $t^{5/2}$ (Woodman, 2007).

Temperature effects Temperature changes cause as well errors in the bias of the output signal. The relationship between the error fluctuations and the temperature changes tends to be highly nonlinear. The use of temperature sensors in order to compensate for this error is a typical solution in MEMS accelerometers(Woodman, 2007).

Calibration errors Calibration errors involve errors in scale factors, alignments and linearities. These errors are only visible when the host object is under acceleration(Woodman, 2007).

A brief explanation of the possible errors in MEMS gyroscopes and accelerometers has been presented. These disadvantages and of course the inertial navigation advantages along with the positive and negative aspects of GPS give opportunity to their integration as explained in the next section.

2.3 GPS/INS Integration

After having analyzed GPS as well as INS, one can find that both systems have complementary characteristics. This section gives an overview of the main GPS/INS integration schemes and architectures along with their main characteristics.

GPS provides position and velocity estimates with bounded errors. However, the magnitude of each one of these errors is relatively not difficult to quantify. As discussed in the introduction, the GPS user may experience some difficulties in a low signal environment where blockage, interference or jamming can be the main problems. This short-term difficulties can be overcome in different ways.

On the other hand we have INS, where the position and velocity estimates are calculated at higher rates (commonly more than 100 Hz) than GPS (commonly less than 20 Hz)and are based on the output of the inertial sensors. These estimates are immune to external interference. However, the estimates depend highly on the output of the sensors; any error with the outputs will lead to unbounded errors in the navigation solution and as I have presented in previous sections inertial sensors have time dependant errors.

The error characteristics then become complementary. Therefore, different architectures and approaches can be implemented when fusing GPS and INS. One example is to use GPS position and velocity estimates to calibrate INS sensors. Another option is to use the high bandwidth attitude, position and velocity INS' estimates as aid during momentary GPS weak signal environment due to blockage, interference or jamming. Since there can be a wide variety of fusion architectures the GPS/INS integration schemes are classified depending on the level of coupling between the two systems. Then, we can find: GPS/INS loosely coupled integration, tightly coupled integration and ultra-tightly (or deep) coupled integration(Gebre-Egziabher, 2007).

2.3.1 Loose GPS/INS Integration

In the loose architecture, the INS and GPS receiver operate as independent navigation systems. Information from the two systems is then blended using an estimator, normally a Kalman filter, to form a final navigation solution and in some cases, when the IMU quality is poor, to estimate the INS errors to correct the gyroscope and accelerometer measurements. A scheme of this architecture is shown in Figure 2.7(Titterton, 2004).

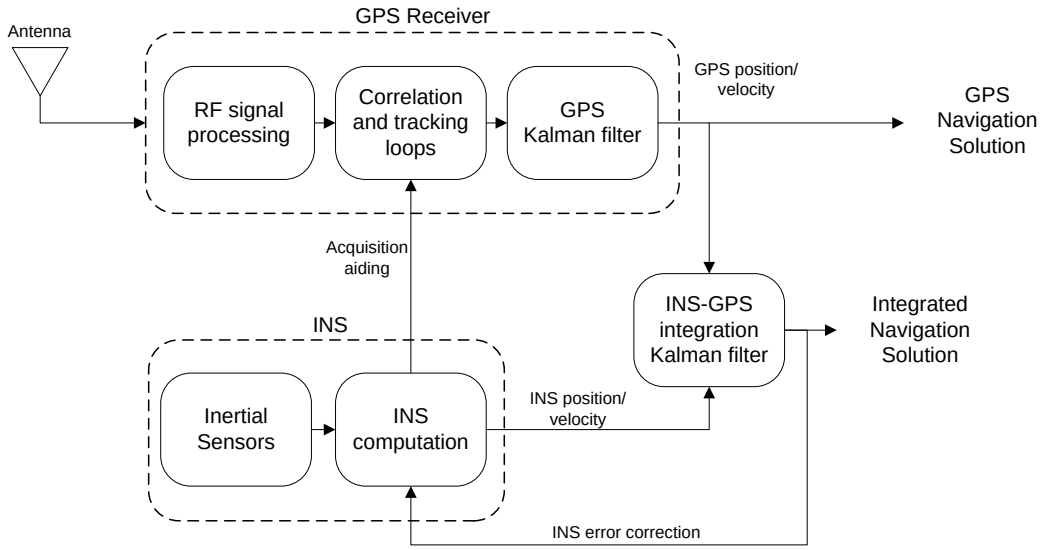

Figure 2.7: GPS/INS loosely coupled integration architecture (Titterton, 2004)

The main advantages of this kind of integration are simplicity and redundancy. This integration can be implemented using any IMU and any GPS receiver and it is common to provide the GPS solution as well as the integrated solution in order to evaluate the integrated one in case any problems can be present(Titterton, 2004).

The purpose of the loose integration is to extract from both systems only the necessary information and blend it together to estimate a new solution. This new solution will include the high bandwidth information from the INS and the GPS bounded errors(Gebre-Egziabher, 2007).

2.3.2 Tight GPS/INS Integration

In tight GPS/INS integration level the INS and GPS receiver are reduced to their basic sensor functions. The GPS receiver provides then the pseudoranges while the INS provides raw acceleration and orientation outputs. In this approach the Kalman filter becomes the most important part of the integration filter. INS error estimates are calculated by means of the GPS pseudoranges and/or pseudorange rates provided by the tracking loop. These

estimates are used to correct the raw INS sensor data which can be used (it is optional in this kind of coupling) to tighten the GPS tracking loops. This enhance allows the GPS receiver to remain in lock with the received signal in high dynamic scenarios. A simplified block diagram of this level of coupling can be seen in Figure 2.8(Titterton, 2004).

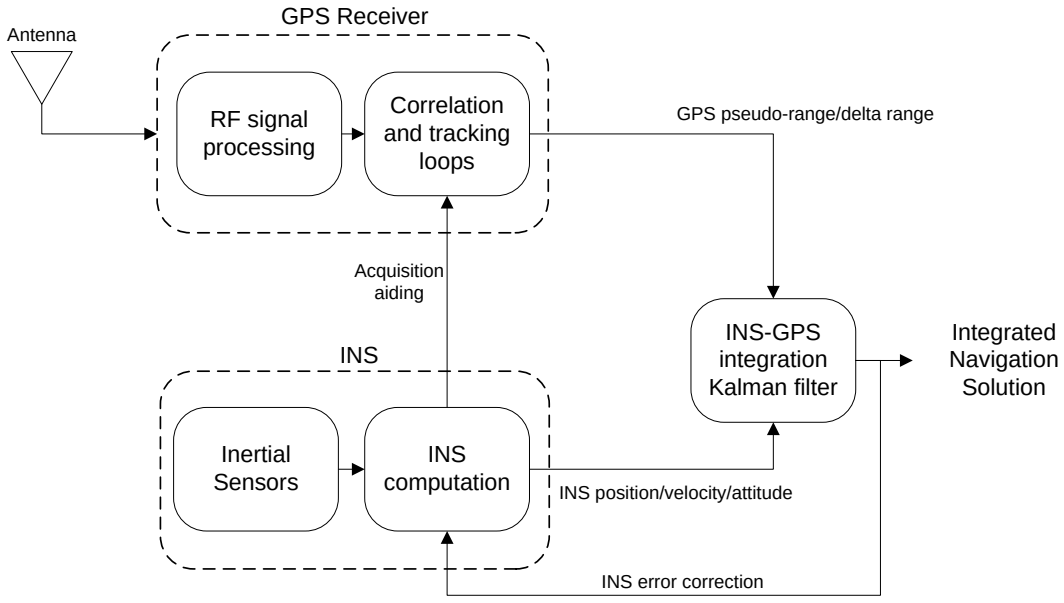

Figure 2.8: GPS/INS tightly coupled integration architecture (Titterton, 2004)

The tightly coupled approach has better accuracy and robustness compared to loosely integration at expense of higher complexity with possible hardware or software changes inside the GPS receiver or the IMU.

2.3.3 Ultra-tight GPS/INS Integration

Ultra-tight integration, also known as deep integration combines GPS signal tracking and INS/GPS integration into a single integration filter, normally a Kalman filter. Ultra-tight integration strategies are currently under development; a simplified block diagram is showed in Figure 2.9.

Tracking the GPS signals together instead of using independent tracking loops, aided by the use of inertial data from the IMU has different benefits(Titterton, 2004):

- Fewer independent quantities are tracked using the same data, therefore the effective signal to noise ratio is improved.
- Multi-path resistance is improved
- Reacquisition of the signal after temporary blockage or interruption can be done faster.
- GPS tracking loops are tightened, reducing the need of a high bandwidth loop filter for high dynamic scenarios. This is an inherent feature in the ultra tight coupling level which differs from the tightly coupled one, where the aid to the tracking loops its optional.

As expected, the complexity is increased in this level of coupling. Computational load and synchronization requirements are necessary for the configuration in order to maintain tracking loop lock(Titterton, 2004).

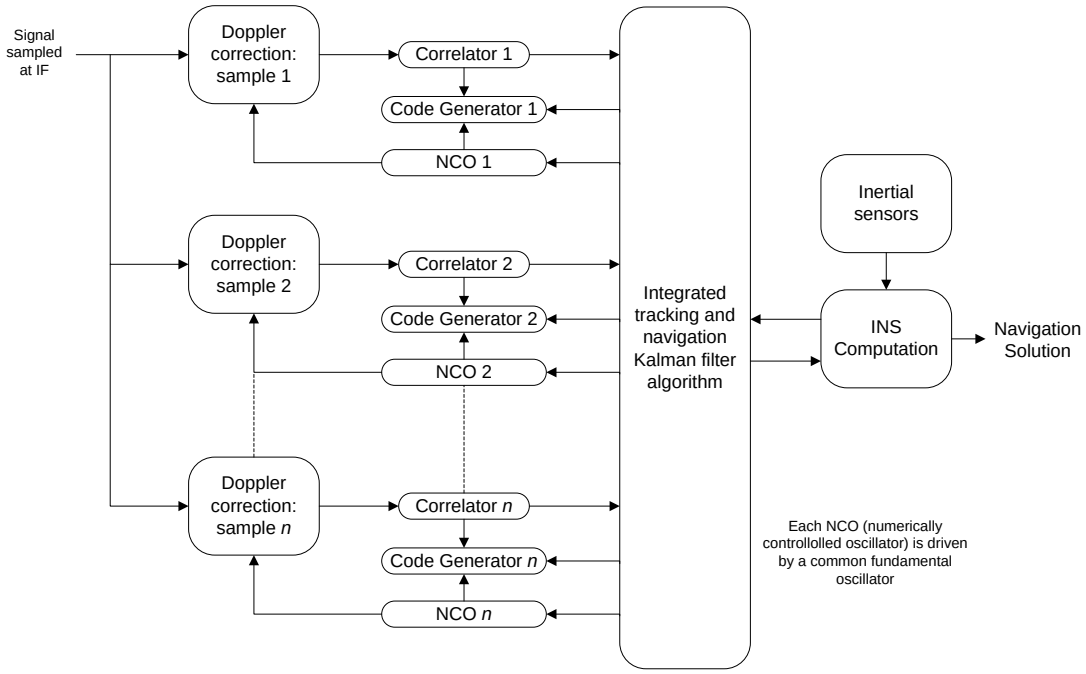

Figure 2.9: GPS/INS ultra-tightly coupled integration architecture (Titterton, 2004)

Although I have presented an overview of the most general coupling levels since they are currently on development stages, a combination of the different implementations of the couplings might be found in certain GPS/INS integrations. Figure 2.10 shows a brief summary of the important implementations depending on the level of coupling.

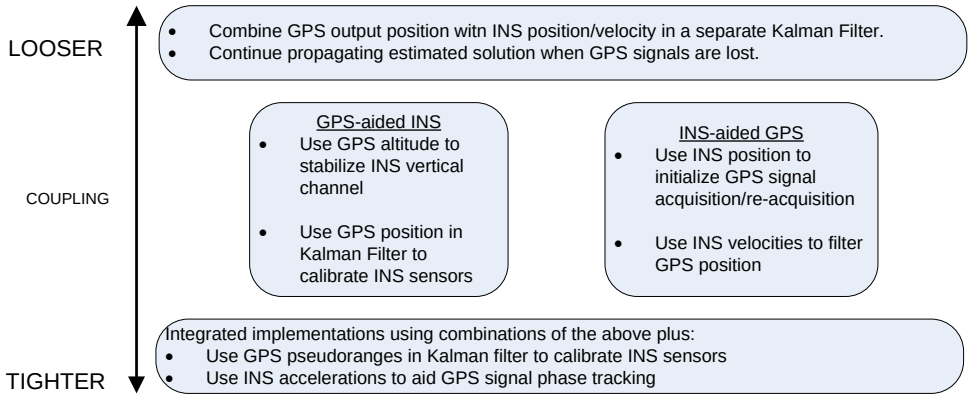

Figure 2.10: GPS/INS implementations depending on the coupling level(Grewal, 2007)

2.4 Kalman Filter

A Kalman filter is an optimal estimator. It infers parameters of interest based on indirect, inaccurate and uncertain observations. The Kalman filter is recursive so that new measurements can be processed as they arrive. It is optimal given the fact that if all noise is Gaussian the Kalman filter minimizes the mean square error of the estimated parameters. The main advantages and reasons of why of this filter is extensively used nowadays are(Kleeman, 1996):

- It gives good results in practice due to optimality and structure.

- It is convenient for real time applications.
- Is is easy to formulate and implement given some basic understanding.

In order to get deeper into the subject we need to explain the state definition. The state of a deterministic dynamic system is the smallest vector that summarizes the past of the system in full(Kleeman, 1996). Having information about this state will allow us, theoretically, to predict the future dynamics and outputs of the deterministic system in the absence of noise.

Assume that the random process to be estimated can be modeled as(Brown and Hwang, 1997):

$$\mathbf{x}_{k+1} = \mathbf{\Phi}_k \mathbf{x}_k + \mathbf{w}_k \tag{2.9}$$

Where $\mathbf{x}_k$ is the process state vector at time t_k, $\mathbf{\Phi}_k$ is the transition matrix that relates $\mathbf{x}_k$ to $\mathbf{x}_{k+1}$ and $\mathbf{w}_k$ is assumed to be a white sequence with known covariance structure.

The measurement of the process can be linearly related as(Brown and Hwang, 1997):

$$\mathbf{z}_k = \mathbf{H}_k \mathbf{x}_k + \mathbf{v}_k \tag{2.10}$$

Where $\mathbf{z}_k$ is the measurement vector at time t_k, $\mathbf{H}_k$ is a matrix giving the noiseless ideal relationship between the measurement and the state vector at time t_k and $\mathbf{v}_k$ is the measurement error assumed to be a white sequence with known covariance having zero crosscorrelation with $\mathbf{w}_k$.

The covariance matrices for the vectors $\mathbf{w}_k$ and $\mathbf{v}_k$ are(Brown and Hwang, 1997):

$$E[\mathbf{w}_k \mathbf{w}_i^T] = \begin{cases} \mathbf{Q}_k, & i = k \\ 0, & i \neq k \end{cases} \tag{2.11}$$

$$E[\mathbf{v}_k \mathbf{v}_i^T] = \begin{cases} \mathbf{R}_k, & i = k \\ 0, & i \neq k \end{cases} \tag{2.12}$$

$$E[\mathbf{w}_k \mathbf{v}_i^T] = \{ \ 0, \quad \text{for all k and i} \tag{2.13}$$

The next step is to assume that we have an initial estimate of the process before the time t_k, called an a priori estimate denoted by $\hat{\mathbf{x}}_k^-$. This shall be assumed to be the best estimate before starting to involve the measurement at time t_k. At the same time we assume to know the error covariance matrix $\mathbf{P}_k^-$ associated with $\hat{\mathbf{x}}_k^-$ depicted in equation 2.14(Brown and Hwang, 1997).

$$\mathbf{P}_k^- = E[\mathbf{e}_k^- \mathbf{e}_k^{-T}] = E[(\mathbf{x}_k - \hat{\mathbf{x}}_k^-)(\mathbf{x}_k - \hat{\mathbf{x}}_k^-)^T] \tag{2.14}$$

The next step is to calculate an updated final estimate $\hat{\mathbf{x}}_k$ for the time point t_k. This is performed using the assumed a priori estimate and the measurement $\mathbf{z}_k$. This updated estimate is calculated weighing the a priori estimate and the noisy measurement according to(Brown and Hwang, 1997):

$$\hat{\mathbf{x}}_k = \hat{\mathbf{x}}_k^- + \mathbf{K}_k(\mathbf{z}_k - \mathbf{H}_k \hat{\mathbf{x}}_k^-) \tag{2.15}$$

Where $\hat{\mathbf{x}}_k$ is the updated estimate and $\mathbf{K}_k$ is the blending factor. The blending factor is known as the kalman gain since its value minimizes the mean square error when calculated with the following equation(Brown and Hwang, 1997):

$$\mathbf{K}_k = \mathbf{P}_k^- \mathbf{H}_k^T (\mathbf{H}_k \mathbf{P}_k^- \mathbf{H}_k^T + \mathbf{R}_k)^{-1} \tag{2.16}$$

The difference $(\mathbf{z}_k - \mathbf{H}_k \hat{\mathbf{x}}_k^-)$ in equation 2.15 is called the measurement residual. This residual shows the discrepancy between the predicted measurement $\mathbf{H}_k \hat{\mathbf{x}}_k^-$ and the actual measurement $\mathbf{z}_k$. Then the covariance matrix $\mathbf{P}_k$ associated with the optimal state needs to be calculated as(Brown and Hwang, 1997):

$$\mathbf{P}_k = (\mathbf{I} - \mathbf{K}_k \mathbf{H}_k) \mathbf{P}_k^- \tag{2.17}$$

The next step in the procedure is to compute the a priori estimate for $\mathbf{x}_{k+1}$ for the time point t_{k+1}(Brown and Hwang, 1997):

$$\mathbf{x}_{k+1}^- = \mathbf{\Phi}_k \hat{\mathbf{x}}_k \tag{2.18}$$

And its associated error covariance matrix:

$$\mathbf{P}_{k+1}^- = \mathbf{\Phi}_k \mathbf{P}_k \mathbf{\Phi}_k^T + \mathbf{Q}_k \tag{2.19}$$

At this point the loop is started again (the Kalman gain is computed again with equation 2.16) since we now have the necessary quantities at t_{k+1} and the measurement $\mathbf{z}_{k+1}$ can be incorporated in order to make a new optimal estimate of the state. This so called Kalman Filter Loop is depicted in Figure 2.11. This algorithm can be broken down into two important procedures: the time update or prediction, comprising block I and the measurement update or correction, comprising the blocks II, III, IV in Figure 2.11, respectively(Welch, 2006).

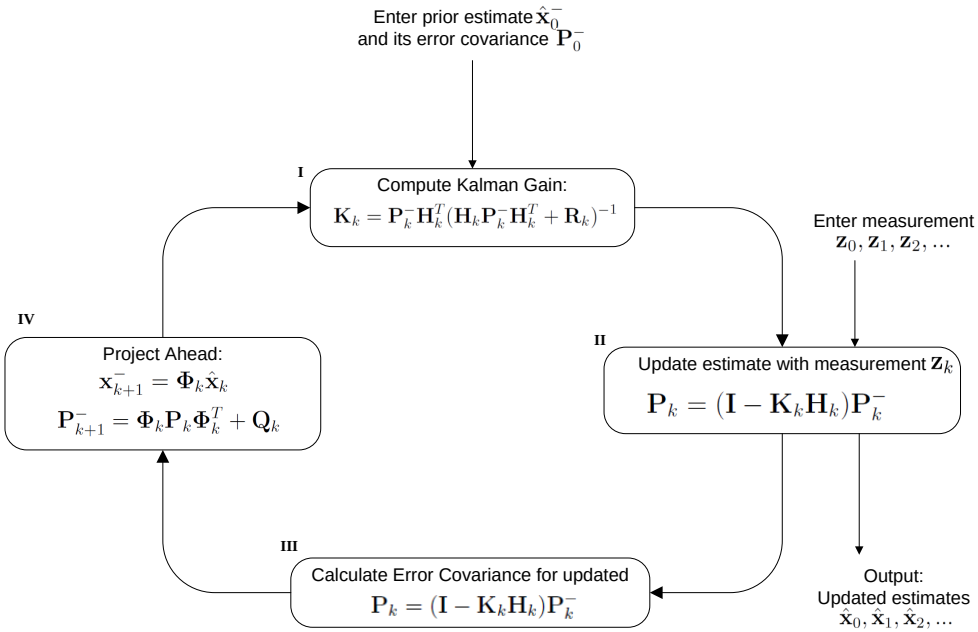

Figure 2.11: Kalman filter loop (Brown and Hwang, 1997)

2.5 Frequency Stability and Signal Noise Analysis

In a later section a signal noise analysis is performed to find the main type of noise perturbing the desired signal. Specifically, partial frequency stability including a noise analysis is performed to a GPS oscillator making it important to give an overview on the theory

behind frequency stability and noise analyses. This section describes then the basic theory behind frequency stability and noise analyses and the main tool, the Allan deviation, used to find the perturbing type noise.

The frequency stability analysis consists in characterizing the phase and the frequency fluctuations of a specific frequency source in a quantitative and standardized manner. This approach takes into account the nominal values, the fluctuations of these values, their dependence on time and environmental conditions(Riley, 2008).

The stability analysis may give information about both the stochastic (noise) and deterministic properties of the source device. It is assumed that the stochastic characteristics of the under test frequency source are constant. However, the analysis may show this last statement is not true and important decisions shall be made then concerning the partition of data in order to have meaningful results(Riley, 2008).

As mentioned above there may exist non-random fluctuations (deterministic properties) and random fluctuations (stochastic properties) which may cause the departure from "true" frequency in the source device. Non-random fluctuations, also called systematic, are the primary cause of the frequency deviation. The most important systematic fluctuations are the frequency offset and the frequency drift. On the other hand, we find the random fluctuations. These deviations are usually characterized statistically. These random fluctuations may be modeled with power law spectral densities where the noise analysis comes into play. In order to have meaningful results regarding the noise analysis, it is a good common practice to remove the deterministic factors such as the frequency drift, offset, temperature sensitivity, etc.(Riley, 2008).

2.5.1 Frequency offset

The estimation of the frequency offset of either phase or frequency data is often necessary when dealing with frequency stability analyses. Frequency offset can be calculated using frequency data. The offset then can be computed simply as the mean of the frequency values(Riley, 2008).

2.5.2 Frequency drift

Once the frequency offset has been removed it is advisable to characterize the frequency drift before analyzing the stochastic noise of the source. Frequency drift refers to the change in frequency due to all external and internal effects. Generally, a fitting trend of the frequency record to a mathematical model is used to compute this systematic drift. This model can be chosen based on some physical basis, a priori information about the types of noise affecting the frequency source or just simply a convenient equation. For this thesis work, a least squares method linear fit is used to deal with the systematic drift(Riley, 2008).

In order to have meaningful results regarding the noise analysis, it is a good common practice to remove the deterministic factors such as the frequency drift, offset, temperature sensitivity, etc.(Riley, 2008).

2.5.3 Power Law Noise

An ideal frequency source is expected to have a constant value in the time domain. When analyzing the source in the frequency domain it is expected to find a single spectral line. The instability of most frequency sources can be modeled by a combination of power-law noises that have a spectral density of their frequency fluctuations in the form $S_y(f) \propto f^{\alpha}$,

where f is the Fourier in Hertz and α is the power law exponent(Riley, 2008). Table 2.3 shows the types of noise and their corresponding value of the power law exponent while Figure 2.12 shows an example of the spectra of the most common types of noise (Riley, 2008).

Noise Type	**Alpha α (Power-law exponent)**
White Phase Modulation	2
Flicker Phase Modulation	1
White Frequency Modulation	0
Flicker Frequency Modulation	-1
Random Walk Frequency Modulation	-2

Table 2.3: Noise Types and their corresponding power-law exponent (Riley, 2008)

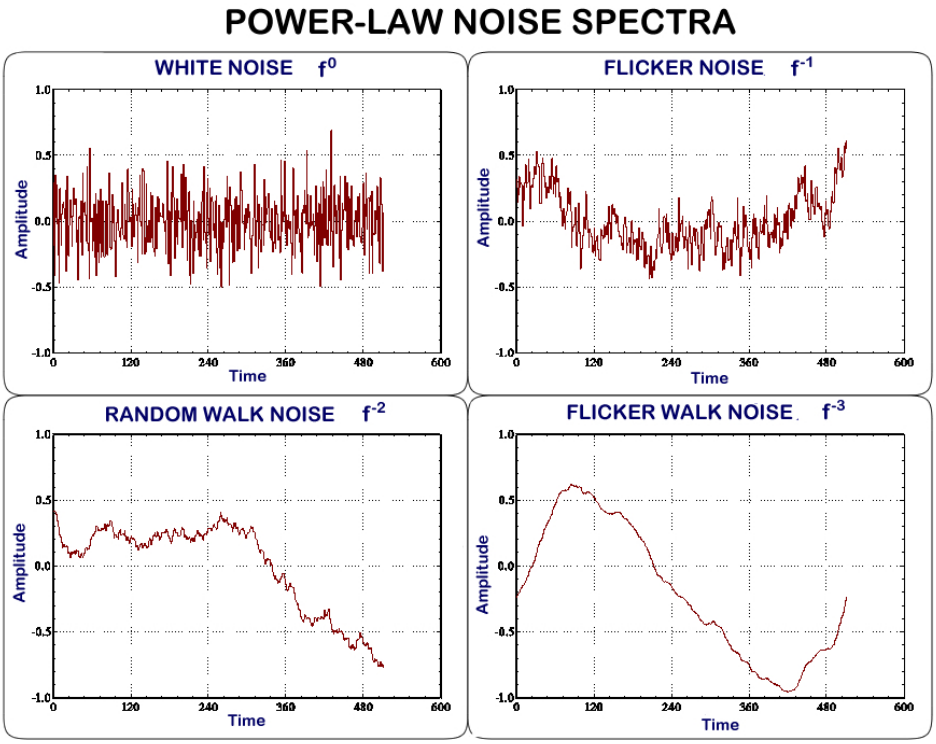

Figure 2.12: Spectra of the four most common types of noise(Riley, 2008)

2.5.4 Sigma-tau plots

The usual way to express the time domain stability of any frequency source is by presenting a sigma-tau plot that shows the measure of frequency stability versus the averaging time. This plot depicts the dependence of stability on the averaging time, the stability value and the type of noise. Depending on the kind of noise, specific slope values μ will result in the plot. As expected, μ and α are related. Figure 2.13 shows the different common types of noise and their different slopes in a log σ versus log τ plot(Riley, 2008).

One can notice from Figure 2.13 that white phase modulation (PM) and flicker phase modulation noise have the same slope. In order to distinguish between these two noise types, a modified sigma plot can be used.

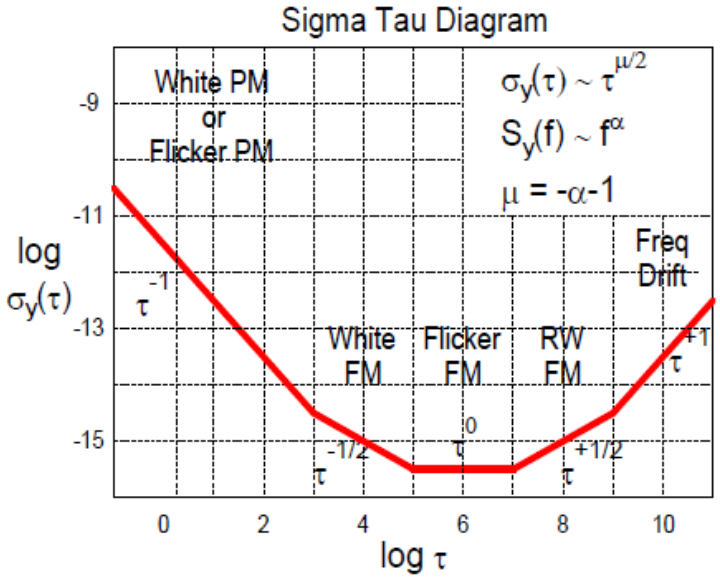

Figure 2.13: Sigma tau plot(Riley, 2008)

2.5.5 Allan Deviation

Characterizing the fluctuations of a frequency source relies in the use of statistical measures. These are 2nd-moment measures of scatter, similar to the standard variance that is used to quantify variations around certain nominal value. Typically, the variations around the mean are calculated as follows(Riley, 2008):

$$s^2 = \frac{1}{N-1}\sum_{i=1}^{N}(y_i - \bar{y})^2 \tag{2.20}$$

The final result is often given as the square root, the so called standard deviation. A problem arises when employing this kind of statistical measurement since it does not converge to a single value for the non-white frequency modulation noises as the number of measurements is increased. Therefore, this statistical tool is not adequate to characterize a frequency source.

In order to counter attack this issue, the Allan variance was developed. The Allan deviation is named after its creator David W. Allan. This deviation uses 2nd differences of frequency to calculate variations and it is convergent to most of the common clock noises. There are several versions of the Allan variance that provide better statistical confidence, and can even distinguish easier the different types of noise. The original Allan variance also called two-sample variance is defined as(Riley, 2008):

$$\sigma_y^2(\tau) = \frac{1}{2(M-1)}\sum_{i=1}^{M-1}[y_{i+1} - y_i]^2 \tag{2.21}$$

Where y_i is the ith of M fractional frequency values averaged over the measurement sampling interval τ.

In terms of phase data, the Allan variance may be calculated as(Riley, 2008):

$$\sigma_y^2(\tau) = \frac{1}{2(N-1)\tau^2}\sum_{i=1}^{N-2}[x_{i+2} - 2x_{i+1} + x_i]^2 \tag{2.22}$$

Where x_i is the ith of the $N = M + 1$ phase values spaced by the measurement interval τ. The result is expressed as the square root, $\sigma_y(\tau)$, the Allan deviation (ADEV).

Another important version of the ADEV is the overlapping Allan deviation. This version makes maximum use of the data set by forming all overlapping samples at each averaging time τ.

Figure 2.14 depicts the comparison between the non-overlapping sampling and its counterpart in order to give a better description about the difference.

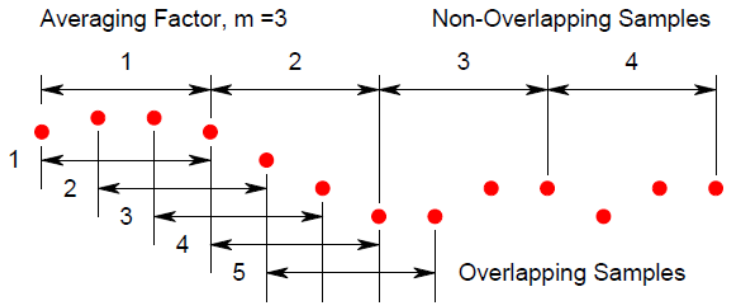

Figure 2.14: Non-overlapping and overlapping sampling comparison(Riley, 2008)

The Overlapping Allan deviation for frequency data is then defined as(Riley, 2008):

$$\sigma_y^2(\tau) = \frac{1}{2m^2(M-2m+1)} \sum_{j=1}^{M-2m+1} \sum_{i=j}^{j+m-1} [y_{i+m} - y_i]^2 \tag{2.23}$$

Where M is the set of frequency measurements for the averaging time $\tau = m\tau_0$, where m is the averaging factor and τ_0 is the basic measurement interval. For phase data the overlapping Allan deviation is defined as(Riley, 2008):

$$\sigma_y^2(\tau) = \frac{1}{2(N-2m)\tau^2} \sum_{i=1}^{N-2m} [x_{i+2m} - 2xi + m + x_i]^2 \tag{2.24}$$

Where $N = M + 1$. The use of overlapping samples involves a trade off. It improves the confidence of the outcome stability measurement but it needs greater computational time. Typically, the overlapping Allan deviation is the first choice when analyzing the frequency stability and noise analysis of any frequency source when not enough information is available(Riley, 2008).

3 Methodology

3.1 Open Loop Approach

On the ultra-tight GPS/INS integration scheme section different important characteristics regarding this architecture were presented. Tracking the GPS signals together aided by the use of inertial data from the IMU is the main key in the architecture. Ultra-tight GPS/INS integration surely requires an increased level of complexity because of the coupling needed. The designer should have certain expertise with the hardware and software of the GPS receiver and specific knowledge on the IMU and GPS synchronization schemes since hardware and software implementations are imperative when applying ultra-tight coupling schemes. The open loop approach presented in this thesis work has the objective of implementing the ultra-tight strategies without going in depth into the hardware and software changes. The received signal from the GPS satellites will go through a Doppler

correction in order to remove the unwanted dynamics. This Doppler correction will induce two important ultra-tight coupling inherent benefits(Titterton, 2004):

- Reduce the need of a high bandwidth loop filter in the tracking loop. A lower bandwidth reduces the noise, improving the effective signal to noise ratio.
- Re-acquisition of the signal after temporary blockage or interruption can be done faster.

The implementation of the open loop approach will keep the frequency of the local oscillator as close as possible to the frequency of the received phase to minimize the phase error in the PLL. This approach is depicted in Figure 3.1:

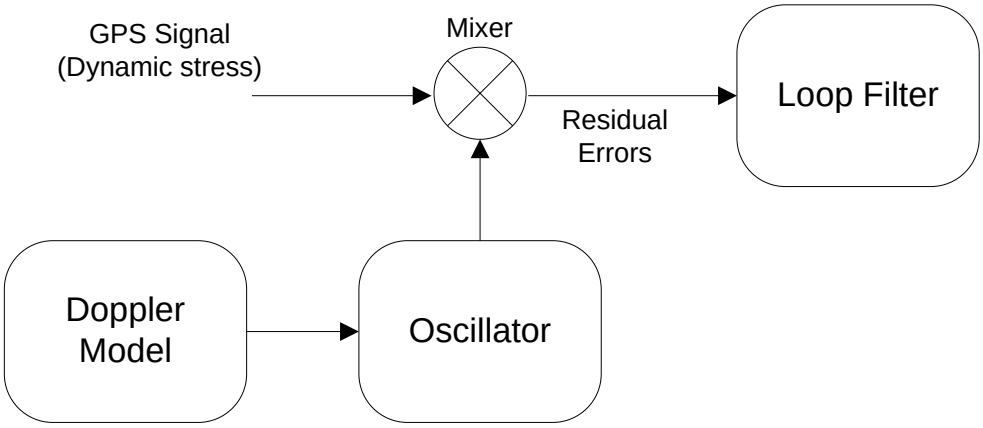

Figure 3.1: Conventional and ultra-tight loop bandwidth

The Doppler correction will allow the receiver to process an almost "dynamic free" signal. The residual dynamics on the GPS signals to be tracked by the carrier tracking loops will mainly depend on the local oscillator and as will be shown later in the errors caused by the IMU measurements. How are these benefits achieved? How are these benefits possible? These questions shall be answered in the following sections.

3.2 Bandwidth and Dynamic Analysis

An analysis on the tracking loop architecture has been done in section 2.1.6. As discussed earlier, the noise bandwidth of the loop filter is one of the most important parameters in the tracking loop design.

First, we have the code tracking loop. The dynamics have less effect on the pseudorandom code than on the carrier since the code Doppler is 1540 times less than on the carrier, therefore, no optimization is needed in this type of tracking loops.

Secondly, and most important we have the carrier tracking loops, where the bandwidth optimization is essential. In low dynamic scenarios the carrier bandwidth requirement tends to be typically of about 5 to 12 Hz. On the other hand, on high dynamic scenarios a bandwidth greater than 18 Hz might be needed. The importance of the noise bandwidth in the loop filter relies in an essential tradeoff. Having a higher bandwidth allows the tracking of GPS signals under high dynamic scenarios. However, higher bandwidth also involves less signal-to-noise ratio, since more thermal noise is introduced into the system(Babu and Wang, 2005).

This problem can be solved as also explained in more detail in the GPS/INS Integration section with the use of an IMU. With the receiver dynamics computed from the IMU data, Doppler information can be extracted in order to remove the dynamic stress on the GPS

signal, therefore, aiding the GPS tracking loops. With the receiver dynamics subtracted from the GPS signal the only thing remaining to track will be the oscillator dynamics which can be achieved with less bandwidth. However, the IMU errors involved in the Doppler model will play an essential role in the dynamics extraction. Figure 3.2 depicts the issue discussed in the last paragraph. It shows the comparison of the loop bandwidth needed between the conventional and ultra-tight receivers.

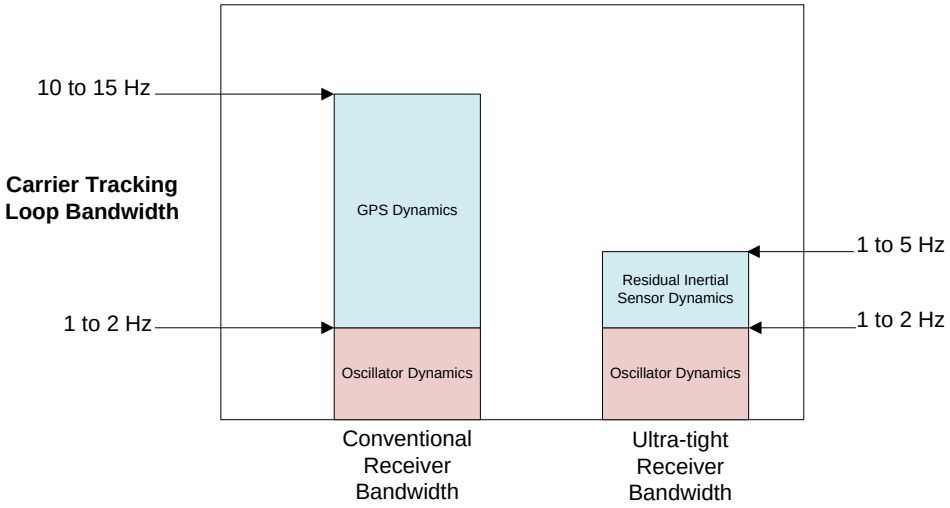

Figure 3.2: Conventional and ultra-tight loop bandwidth

In order to track a GPS signal a threshold needs to be set according to the statistical properties of the signal and the thermal noise. The 2 most important factors to consider then for setting the threshold are the expected dynamics and the loop bandwidth.

The performance of a tracking loop can be determined by measuring the phase error. This phase error includes the thermal noise as well as the dynamic stress. The 3-sigma phase errors that a carrier tracking loop can tolerate is given by(Kaplan, 2006):

$$3\sigma_{PLL} = 3\sigma_t + \theta_e < 45^\circ \tag{3.1}$$

Where σ_t is the 1-sigma phase error due to thermal noise, θ_e is the dynamic stress error and 45° is the threshold below which the signal is assumed to be lost.

The thermal noise error can then be calculated as(Kaplan, 2006):

$$\sigma_t = \frac{360}{2\pi}\sqrt{\frac{B_n}{c/n_0}(1+\frac{1}{2Tc/n_0})} \tag{3.2}$$

And the dynamic stress is given by(Kaplan, 2006):

$$\theta_e = 0.2809\frac{\vec{a}}{B_n^2}(deg) \tag{3.3}$$

Where:

B_n is the loop bandwidth in Hz

c/n_0 is the carrier to noise ratio

T is the pre-detection integration time

$\vec{a}$ is the line-of-sight acceleration between the satellite and the GPS receiver in m/s^2

Figure 3.2 shows both the thermal noise and dynamic stress as a function of the bandwidth assuming a typical 1ms pre-detection time, a carrier to noise ratio of 27.5 dB-Hz and 0.5g dynamics(Babu and Wang, 2005).

It is important also to observe that as the bandwidth increases the thermal noise takes more importance in the total error calculation due to the fact that the thermal noise is increased as the loop bandwidth is increased. Figure 3.3 shows the influence of dynamics on the required noise bandwidth to mantain a certain threshold. As explained before, higher dynamics require higher loop bandwidth. One can notice the influence of the dynamics in the tracking loop performance. Thus, making it imperative to remove them.

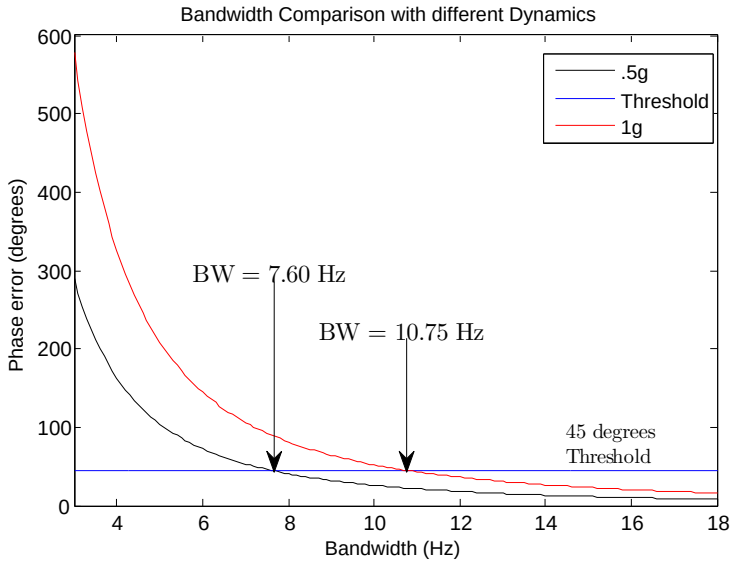

Figure 3.3: Dynamic stress and thermal error

3.3 Doppler Analysis

From the previous section we can conclude that the receiver dynamics need to be removed. How does this Doppler effect affects the GPS carrier frequency? How does the IMU derived information come into play? This section will make an analysis on the doppler effect.

The Doppler effect, named after the Austrian physicist Christian Doppler, by definition is the change in frequency of a wave for an observer moving relative to the source of the wave. The Doppler itself is a clear quantitative sign of the relative dynamics experienced by the GPS radio frequency carrier.

In order to begin with the analysis let's start with the carrier dynamics, assuming the pseudorandom code is already tracked and we can discard it for simplicity purposes. The signal at the carrier tracking loop is given by(Babu and Wang, 2005):

$$y(t) = A\sin(2\pi(f_{rel-vel} + f_{clk})t + \phi) \tag{3.4}$$

Where:

A is the amplitude of the GPS signal

$f_{rel-vel}$ is the doppler frequency caused by the receiver dynamics

f_{clk} is the doppler shift due to the receiver's clock

ϕ is the carrier phase at the phase detector

To track the signal from equation 3.4, the NCO at the traking loop generates two signals we have already discussed in section 2.1.6: the in-phase(I) and quadrature(Q) signals. The

signals are shown in Figure 2.1. In a conventional receiver, the phase discriminator is in charge of generating the necessary corrections for the NCO. However, in the new open loop approach, the extracted IMU doppler data takes a more important role in the correction management besides the phase discriminator correction. Mathematically speaking, when calculating the receiver dynamics from the IMU we generate two new signals given by(Babu and Wang, 2005):

$$y_I(t) = \sin(2\pi \hat{f}_{IMU} t + \theta) \tag{3.5}$$

$$y_Q(t) = \sin(2\pi \hat{f}_{IMU} t + \theta + 90^\circ) \tag{3.6}$$

It is important to mention that $\hat{f}_{IMU}$ is not the true doppler since it is perturbed by the residual biases in the inertial sensors. Therefore:

$$\hat{f}_{IMU} = f_{IMU} + f_{bias} \tag{3.7}$$

The true doppler frequency is then equal to the receiver dynamics $f_{rel-vel}$ and can be calculated as(Babu and Wang, 2005):

$$f_{IMU} = f^{tx}(1 - \frac{\upsilon_{rel}\vec{a}}{c}) = f_{rel-vel} \tag{3.8}$$

Where:
$\hat{f}_{IMU}$ is the Doppler frequency generated from the IMU data
f_{IMU} is the true Doppler frequency
f_{bias} is the residual bias from the IMU inertial sensors
f^{tx} is the transmitted GPS frequency
υ_{rel} is the relative velocity between the satellite and the IMU
$\vec{a}$ is the line-of-sight vector
c is the velocity of light

The Doppler correction then takes place when the signal from equation 3.4 is multiplied by the in-phase 3.5 and quadrature 3.6 signals, respectively; since we want to remove the doppler frequency effects with the IMU dynamics. The resulting signal is then defined as:

$$yy_I(t) = cos(2\pi(f_{GPS} - \hat{f}_{IMU})t) \tag{3.9}$$

$$yy_Q(t) = cos(2\pi(f_{GPS} - \hat{f}_{IMU})t + 90^\circ) \tag{3.10}$$

Where in equations 3.9 and 3.10 f_{GPS} is defined as:

$$f_{GPS} = f_{clk} + f_{rel-vel} \tag{3.11}$$

f_{clk} is the receiver clock Doppler shift due to the oscillator dynamics and $f_{rel-vel}$ is the relative velocity between the satellite and the receiver. Notice that in equations 3.9 and 3.10 only the low frequency components generated by the mixing process are considered since the loop filter removes the high frequency components.

After substituting equations 3.7 and 3.11 into equations 3.9 and 3.10 we finally obtain the corrected Doppler I and Q signals:

$$yy_I(t) = cos(2\pi(f_{clk} - f_{bias})t) \tag{3.12}$$

$$yy_Q(t) = cos(2\pi(f_{clk} - f_{bias})t + 90^\circ) \tag{3.13}$$

Finally both signals are integrated over the integration period T and we end up with(Babu and Wang, 2005):

$$E[I] = \frac{A}{2f_{residual}} cos(f_{residual}(k+1)T) - cos(f_{residual}kT) \tag{3.14}$$

$$E[Q] = \frac{A}{2f_{residual}} sin(f_{residual}(k+1)T) - sin(f_{residual}kT) \tag{3.15}$$

Where:

$$f_{residual} = f_{clk} - f_{bias} \tag{3.16}$$

And E is the expectation operator.

We can conclude then from equation 3.16 that the effective Doppler to track after the correction $f_{residual}$ is comparatively less than the Doppler at the first received signal depicted in equation 3.4. Having reduced the doppler effect we can then expect that less bandwidth on the loop filter will be needed if aiding is implemented. The proof presented in the above equations is only possible considering the biases in the inertial sensors are small enough, meaning high quality inertial sensors are used and the clock in the GPS is stable. Having low accuracy inertial sensors or unstable clocks will result in a inefficiency and the implemented ultra-tight strategies then lose their advantage.

Assuming accurate inertial sensors and stable clocks are used in the implementation, the next step is to create a Doppler model in order to analyze in depth the different roles played by the satellite, receiver and clock dynamics.

3.4 Doppler Model

The Doppler model presented in this thesis work consists of several major aspects: the satellite, the receiver, the clock dynamics as well as signal propagation effects due to atmospheric conditions. A different approach is given to all of them, since they play an important part in the Doppler calculation. Equation 3.8 in the previous section can be further developed as:

$$f_{IMU} = f^{tx}(1 - \frac{(V_{rx} - V_{sat})\vec{a}}{c}) = f_{rel-vel} \tag{3.17}$$

Where V_{sat} is the satellite's velocity and V_{rx} is the GPS receiver velocity. From equation 3.17 we can observe the importance in calculating V_{sat} and V_{rx} accurately, since they describe the satellite and receiver dynamics. The third component, the clock dynamics is included in the $f_{residual}$, where it is important to show that its nominal value is almost negligible and even some modeling approach can be pursued.

3.4.1 Satellite Dynamics

One of the essential components as explained above is the calculation of V_{sat}. This velocity can be calculated in any Earth reference frame, such as Earth-Centered-Earth-Fixed (ECEF). In order to compute V_{sat} two important concepts shall be introduced.

First, the broadcast ephemeris inside the navigation message discussed in section 2.1.2 comes into play once again. In the broadcast ephemeris important Keplerian parameters with correction terms are sent to the GPS receiver in order to calculate the broadcast orbits. These parameters are shown in Table 3.1.

Second, the Interface Control Document (ICD-GPS-200c). This document was expedited by the U.S. Coast Guard Navigation Center in agreeement with several companies

Parameter	Definition
t_{0e}	Reference epoch of ephemeris
$\sqrt{a}$	square root of semi-major axis
e	Eccentricity
i_0	Inclination angle (at time t_{0e})
Ω_0	Longitude of ascending node (at weekly epoch)
ω	Argument of perigee(at time t_{0e})
M_0	Mean anomaly(at time t_{0e})
$\dot{i}$	Rate of change of inclination angle
$\dot{\Omega}$	Rate of change of longitude of ascending node
Δn	Mean motion correction
C_{uc}	Amplitude of cosine correction to argument of latitude
C_{us}	Amplitude of sine correction to argument of latitude
C_{rc}	Amplitude of cosine correction to orbital radius
C_{rs}	Amplitude of sine correction to orbital radius
C_{ic}	Amplitude of cosine correction to inclination angle
C_{is}	Amplitude of sine correction to inclination angle

Table 3.1: GPS ephemeris parameters

developing GPS in 1983. From that time it has been continously updated. The ICD-GPS-200c defines the requirements related to the user interface between the space segment and the user segment in GPS. The ICD-GPS-200c contains among other important features an algorithm to calculate the ECEF satellite position from the broadcast ephemeris. However, no algorithm is provided in order to calculate the satellite velocity, thus, several options might be implemented in order to calculate V_{sat}(USCGNV, 1993).

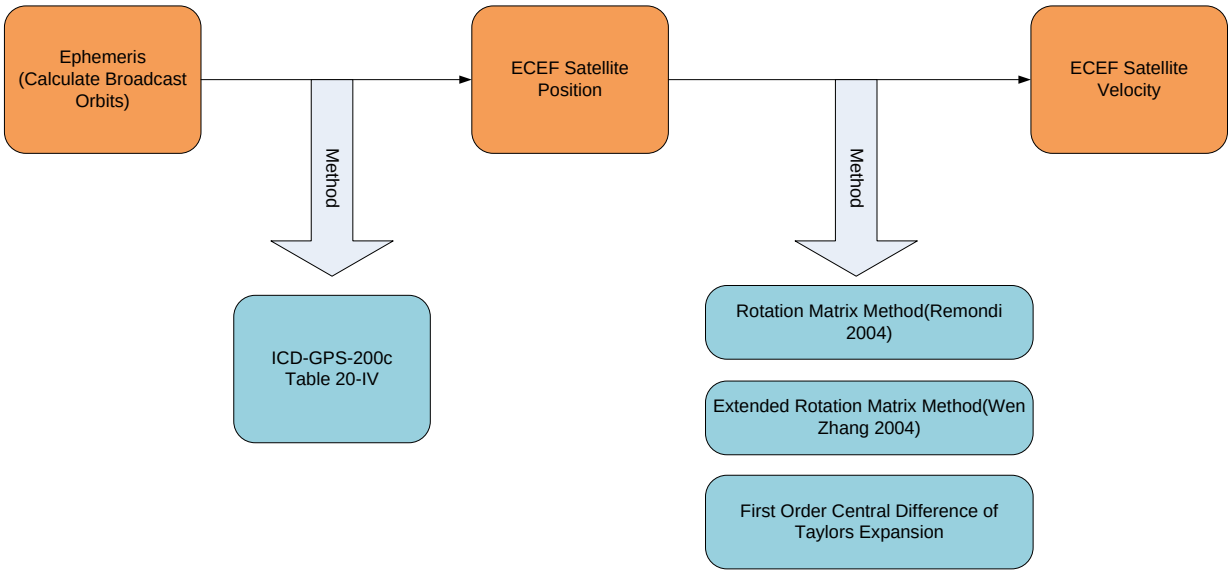

Figure 3.4: Block diagram for the calculation of the satellite's ECEF velocity

In summary (and depicted in Figure 3.4), from the broadcast ephemeris parameters the broadcast orbits are computed. The next step is to calculate the ECEF satellite position applying the algorithm from ICD-GPS-200c, the derivation of this algorithm is beyond the scope on this thesis work, the interested reader can check reference(USCGNV, 1993) for more information. Once the position is calculated, one can proceed to implement one of the following algorithms to obtain the satellite's ECEF velocity:

- Rotation Matrix Method
- Extended Rotation Matrix Method
- First Order Central Difference of Taylors Expansion

Rotation Matrix Method This method relies in the derivation of a set of equations to calculate the velocity and acceleration using the Keplerian elements and correction terms included in the broadcast ephemeris. How to derive the equations are beyond the scope of this thesis work, however, the algorithm is presented in (Remondi, 2004) with further explanation on the Keplerian elements for the interested reader. The final equations to calculate the velocity are given by:

$$\dot{x}_k = -x_p\dot{\Omega}_k \sin\Omega_k - y_p(\dot{\Omega}_k \cos\Omega_k \cos i_k - \dot{i}_k \sin\Omega_k \sin i_k) + \dot{x}_p \cos\Omega_k - \dot{y}_p \sin\Omega_k \cos i_k \quad (3.18)$$

$$\dot{y}_k = x_p\dot{\Omega}_k \cos\Omega_k - y_p(\dot{\Omega}_k \sin\Omega_k \cos i_k + \dot{i}_k \cos\Omega_k \sin i_k) + \dot{x}_p \sin\Omega_k + \dot{y}_p \cos\Omega_k \cos i_k \quad (3.19)$$

$$\dot{z}_k = y_p\dot{i}_k \cos i_k + \dot{y}_p \sin i_k \quad (3.20)$$

Where:
$\dot{x}_k$, $\dot{y}_k$ and $\dot{z}_k$ are the x-ECEF, y-ECEF and z-ECEF velocities, respectively
x_p and y_p are the in-plane x and y positions, respectively
$\dot{x_p}$ and $\dot{y_p}$ are the in-plane x and y velocities, respectively
Ω_k is the corrected longitude of node
i_k is the corrected inclination

Extended Rotation Matrix Method The extended rotation matrix method is similar to the rotation matrix method. The difference relies in the calculation of the rate of change of the true anomaly $\dot{\nu_k}$. The unextended version presents an equation for the rate of change of the true anomaly based on Kepler's second law (the radius vector sweeps out equal areas in equal time on an orbit). However, this will yield an error when the time from ephemeris epoch t_k is not equal to zero. The larger the value of t_k, the larger the satellite ECEF velocity error.

The extended version then introduces a new equation based on the derivative of the mean anomaly M_k and the derivative of the eccentric anomaly E_k, suppressing then the error. The true anomaly is then given by(Zhang, 2009):

$$\dot{\nu}_k = a^2 \frac{\sqrt{1-e^2}}{1 - e\cos E_k} \quad (3.21)$$

While in the rotation matrix method is given by(Remondi, 2004):

$$\dot{\nu}_k = a^2 \frac{n\sqrt{1-e^2}}{r_k^2} \quad (3.22)$$

Where:
$\dot{\nu}_k$ is the rate of change of the true anomaly
E_k is the eccentric anomaly
e is the eccentricity
a is the semi-major axis

n is the corrected mean motion

r_k is the corrected radius

The derivation of the equations as well as a further explanation on the Keplerian parameters are beyond the scope of this thesis work, however the interested reader can consult(Zhang, 2009) for more information. The velocity equations for the extended version are the same than the ones for the rotation matrix method, having in mind that the true anomaly is computed in a different way.

First Order Central Difference of Taylors Expansion This method comes as an option due to the complexity and computational load that may arise from the previous two methods. The straight forward method of differentiating the ECEF satellite positions to obtain the ECEF velocity may lead to a large error, since the broadcast ephemeris have an accuracy of approximately $\pm$ 1 to 5 meters. Thus, the resultant velocity will be very noisy because of the differentiation process. However, another velocity algorithm that can be implemented relies in the use of the first-order central difference of a Taylor series approximation(Zhang, 2006):

$$\dot{\vec{r}}_{ECEF}(t) = \frac{\dot{\vec{r}}_{ECEF}(t + \Delta t) - \dot{\vec{r}}_{ECEF}(t - \Delta t)}{2\Delta t} \tag{3.23}$$

Where:

$\vec{r}_{ECEF}$ is the satellite's position in the ECEF system

$\dot{\vec{r}}_{ECEF}$ is the satellite's velocity in the ECEF system

t is the time of the calculation epoch

Δt is the time interval

Which algorithm to implement depends on the error tolerance and computer load availability; however, as will be shown in the results, these 3 algorithms have similar errors. The errors from the three methods are analyzed in the results section where the Doppler frequency due to the satellite motion will be calculated and an error from the calculation will arise due to the error in the velocity calculation. This error will then be analyzed in an error budget.

3.4.2 Receiver Dynamics

The next component to compute is V_{rx}. In a conventional GPS receiver this component is one of the common measurements found inside the tracking loop. However, the receiver does not have enough bandwidth to aid the PLL properly. Therefore, in this model the V_{rx} component is going to be calculated with the use of a high quality IMU.

For this component we have available data from an IMT40 IMEGO IMU. The IMU was mounted on top of an industrial robot which performed programmed movements according to a reference position file. The acceleration data will go through a simple strapdown algorithm resulting in the desired velocity. As an attempt to have better velocity estimates, the data will be processed using a Kalman filter in order to merge known data (such as when the robot in motion stops for a few seconds) with the velocity measurements.

Finally, the velocity estimates will be used to calculate the Doppler frequency due to the receiver dynamics. This Doppler frequency is then compared with ideal values calculated from the programming file in order to find the errors in the Doppler calculation and add them to the error budget. It is important to mention that this calculated Doppler frequency will be perturbed by the explained errors in sections 2.2.4 and 2.2.6. Therefore, they will have a large influence in the Doppler calculation.

3.4.3 Clock Dynamics

In the bandwidth and dynamic analysis as well as in the Doppler analysis we concluded that the clock dynamics should be small enough to be tracked without problems by the PLL in the GPS receiver. For this thesis work, available data from a free running oscillator of a JAVAD receiver will be analyzed using the frequency stability and noise analysis strategies presented in section 2.5. This analysis will then give an insight on the previous conclusions explained in the Doppler analysis.

On the other hand, a smaller error induced by the clocks on-board the satellites need to be considered. A literature study on this effect has been performed.

3.4.4 Atmospheric effects

Signal propagation problems will arise from the properties of the ionosphere and the troposphere as already discussed in section 2.1.4. This signal propagation issues are added to the error budget. A literature study on these components and their influence was performed.

4 Results

4.1 Satellite Dynamics

In section 3.4.1 I have presented three different methods in order to deal with the satellite dynamics, in other words, to calculate the ECEF satellite velocity. A literature study has been carried out to analyze the three methods to realize their potential errors when dealing with the Doppler calculation.

The three methods were compared with the velocities calculated by the National Geodetic Service (NGS) using the SP3 precise ephemeris, these velocities can be downloaded from the NGS website as explained in reference (Marshall, 2002).

Velocity components from NGS SP3 precise positions were downloaded specifically for PRN07 on August 20th, 2002 from 22:10:01 to 22:19:10. This information will then work as the reference data to compare the rotation matrix method, the extended rotation matrix method and the first order central difference of a Taylor series(Zhang, 2009). For further information on the implementation of the three methods, the interested author can read (Remondi, 2004),(Zhang, 2009) and (Zhang, 2006). Table 4.1 summarizes the studied results:

Method	**Velocity Accuracy**	**Doppler Accuracy**
Rotation Matrix Method	$\pm 1 dm/s$	$\pm .52515 Hz$
Extended Rotation Matrix Method	$\pm 1 mm/s$	$\pm .0052515 Hz$
Taylors Expansion Method	$\pm 1 mm/s$	$\pm .0052515 Hz$

Table 4.1: Methods accuracy comparison

In can be inferred from Table 4.1 that the extended rotation matrix is more accurate than the non-extended version due to the fact that the later does not correct the semi-major axis a which changes over the time epochs t_k.

The most interesting aspect is that the first-order central difference of Taylors expansion's results are close to the NGS SP3 ephemeris by better than $\pm 1 mm/s$. These interesting results are associated with the fact that the orbit error positions are not Gaussian white; systematic bias and correlated errors of the satellite ECEF positions due to

errors in the broadcast ephemeris are mitigated through the differentiation process (Zhang, 2006).

We can conclude then that the optimal step-by-step implementation for the satellite dynamics for real time applications should be:

1. Calculate the ECEF position implementing the ICD-GPS-200c algorithm.

2. Calculate the satellite ECEF velocity implementing the first-order central difference of Taylors expansion since it requires les computational load and has practical and simplicity advantages over the other two methods when talking about real time applications.

It is important to mention that there will exist an error of $\pm.0052515Hz$ that shall be taken into account in the Doppler model error residuals.

4.2 Receiver Dynamics

For this section, data available from an IMEGO IMT40 IMU was analyzed. This data was obtained after mounting the IMU on a robot at the Onsala Space Observatory. The robot was programmed to perform specific movements while GPS data and IMU data were recorded. Fourteen runs using the same specific movement's program file are available. The data was processed and analyzed using the Matlab©software environment. The data included sensor measurements up to 50 seconds of programmed movement. The programming file for the robot consists on east, north and vertical coordinates as well as a time interval to determine the amount of time the robot should hold in each coordinate. This interval time was .1 seconds.

Ideal Robot Velocity Applying simple physics to the available programming file coordinates and times, a true ideal velocity was calculated in order to use it as a reference.

IMU Calculated Velocity The available acceleration measurements from the IMT40 IMEGO's IMU were used to calculate the velocity on the east, north and vertical axes. An integration scheme, based on the strapdown algorithm was implemented in order to compute this velocity.

Kalman Output Velocity A Kalman filter was implemented in this case in order to merge known robot motion information along with the acceleration measurements obtained from the IMU. The known information consists on the .1 seconds where the robot should stay in a determined coordinate, where we can assume that the velocity for exactly that time interval is equal to zero. The measurements consist in the calculated velocity, explained in the prior paragraph.

Figures 4.1, 4.2 and 4.3 show the IMU calculated velocity compared with the ideal robot velocity for the east, north and vertical components for one of the runs. One can observe that the IMU calculated velocity shows the ongoing errors from the inertial sensors as they drift away with time in the different axes.

Figures 4.4, 4.5 and 4.6 show the Kalman output after merging the known information where the robot velocity is equal to zero and the data from the IMU strapdown algorithm.

The next step is to calculate the rms Doppler errors for both the IMU calculated velocity and the Kalman output. Figures 4.7 and 4.8 show the rms Doppler errors, respectively.

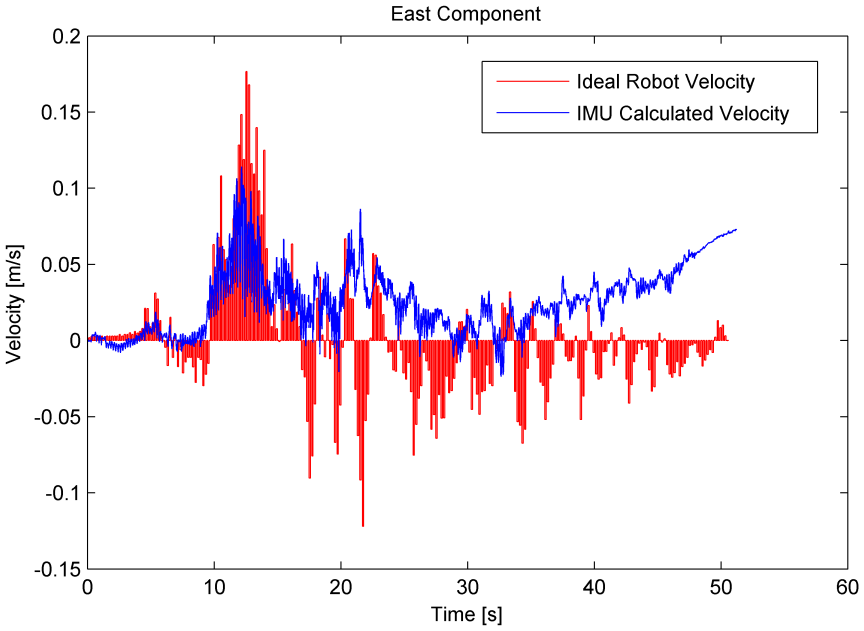

Figure 4.1: Velocity calculations in the east component

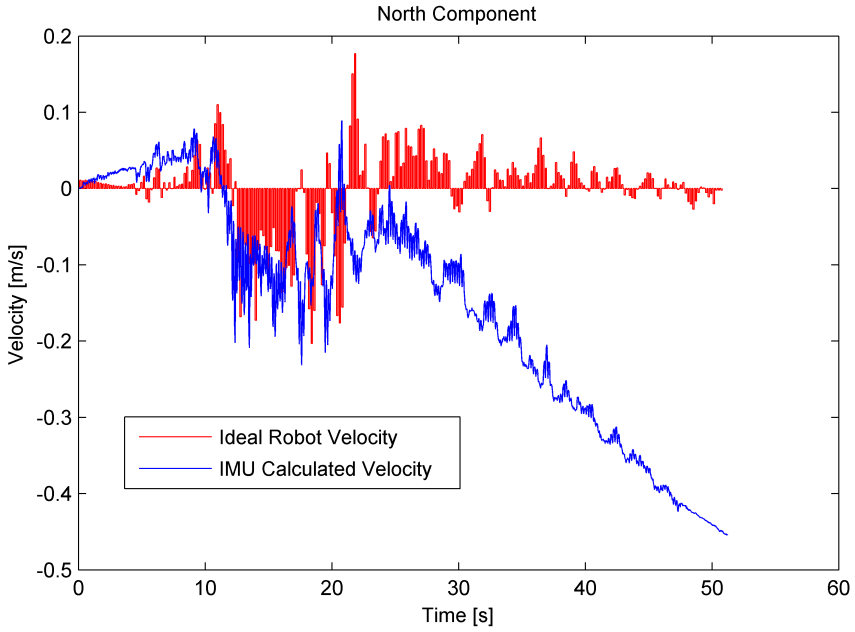

Figure 4.2: Velocity calculations in the north component

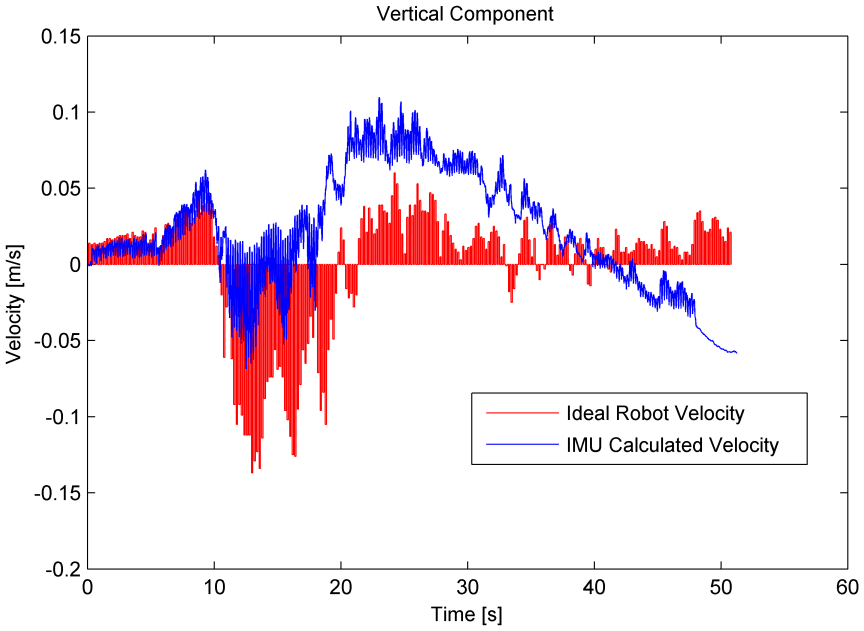

Figure 4.3: Velocity calculations in the vertical component

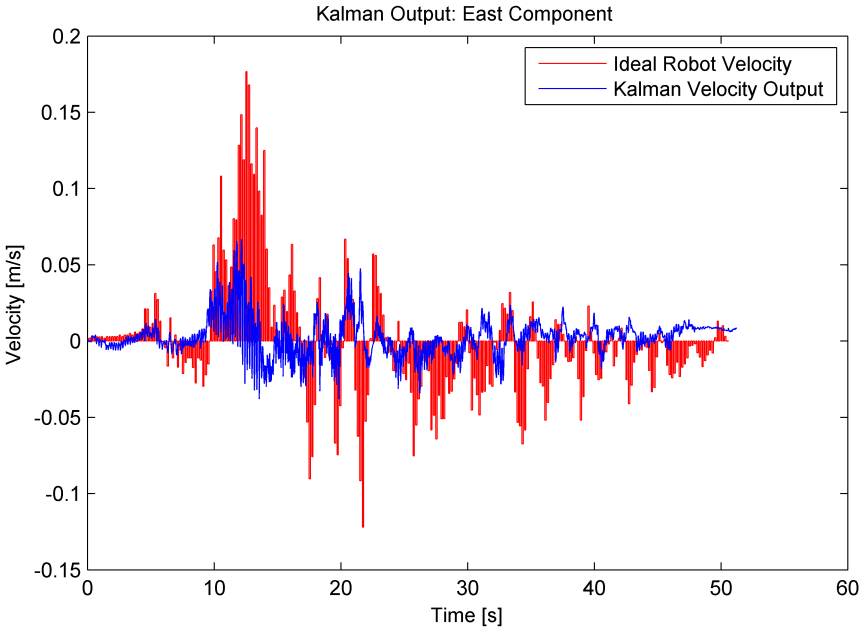

Figure 4.4: Kalman velocity output for the east component

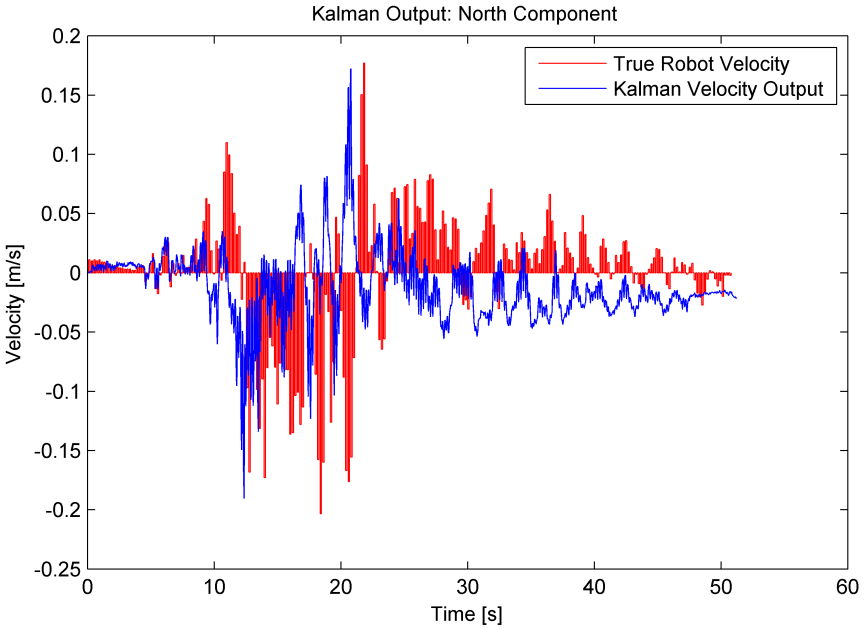

Figure 4.5: Kalman velocity output for the north component

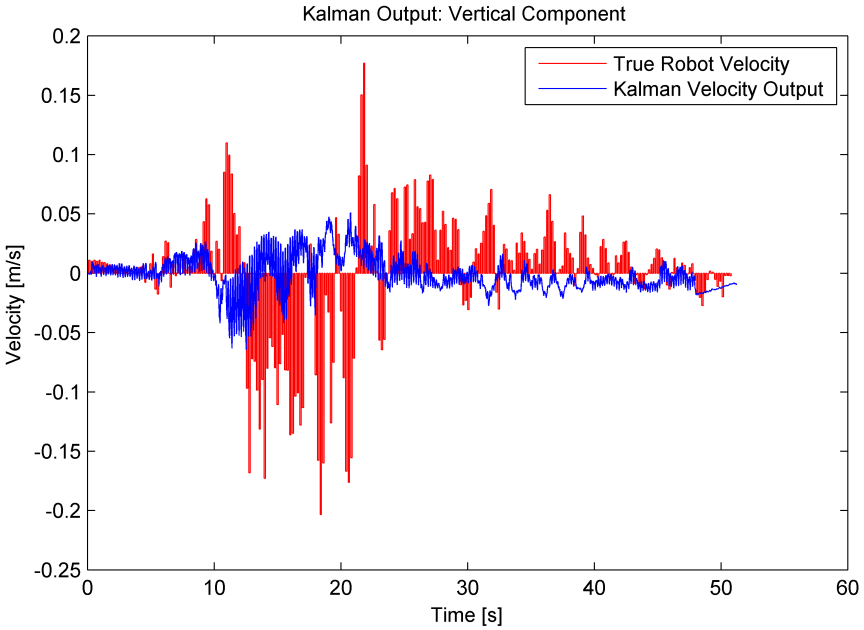

Figure 4.6: Kalman velocity output for the vertical component

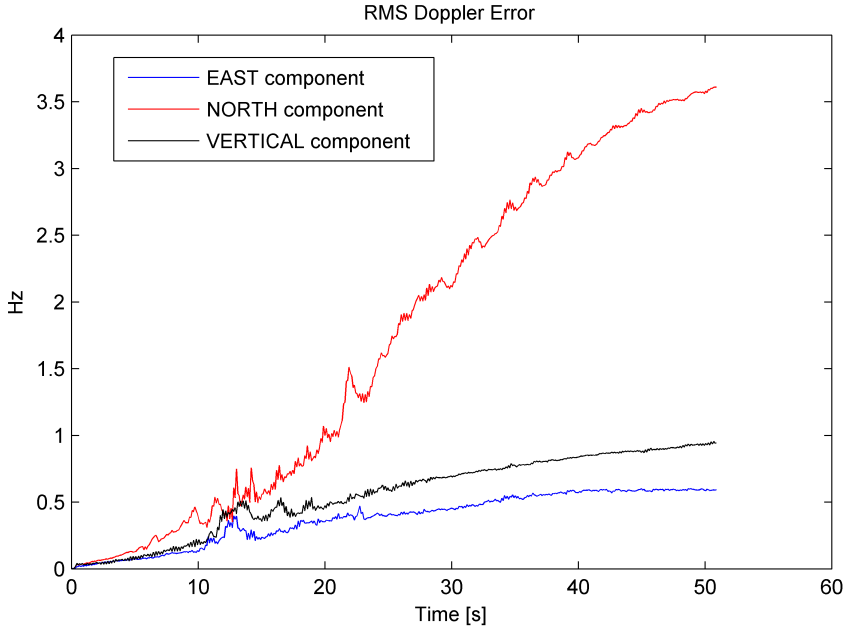

Figure 4.7: RMS Doppler error caused by the receiver dynamics

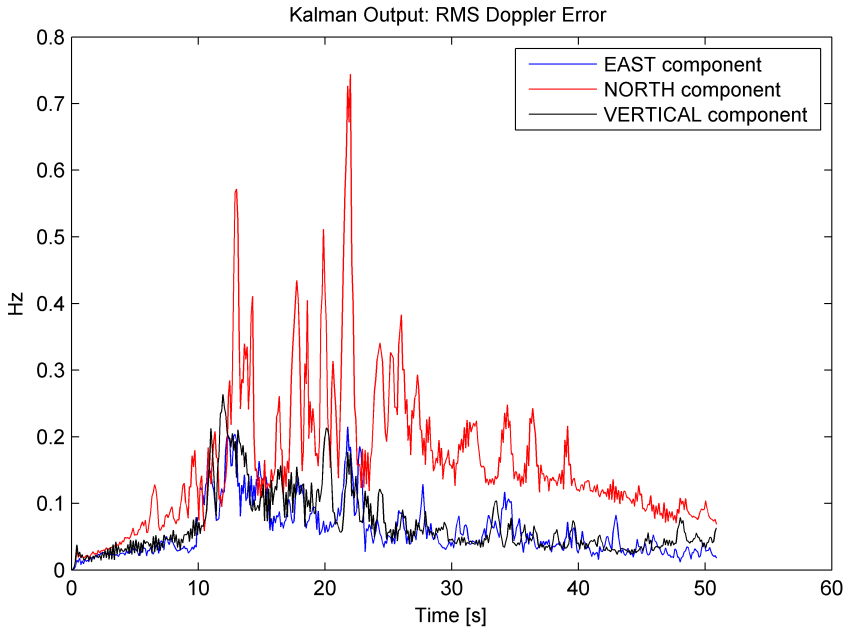

Figure 4.8: RMS Doppler error caused by the receiver dynamics for the Kalman velocity output

As mentioned earlier, we can observe from Figure 4.7 the impact of the inertial sensors since they have time dependant errors. However, the implementation of a navigation algorithm, in this case a simple Kalman filter merging known information and sensor measurements, shows to be a wise approach since it reduces the errors significantly.

It is important to mention that the IMU data available consists of only 50 seconds of information. A good idea for the future would be to collect data from the IMU for longer periods of time as well as to perform the experiment using faster vehicles to analyze the velocity as well as the long term time influence.

For the error budget the errors from Figure 4.7 are the ones taken into account since the Kalman filter method requires apriori knowledge about the velocity, which in real time applications is not possible to obtain.

4.3 Receiver clock

In this section data was obtained from a Time Interval Counter (TIC). The measurements in nanoseconds were taken every second between the GPS receiver's 1 pulse per second (PPS) output and 1 PPS created from the Swedish national time scale UTC(SP). The UTC SP is a realisation of the Coordinated Universal Time (UTC) maintained using atomic clocks, cesium clocks and hydrogen masers, therefore, making it an optimal time reference. The obtained measurements were then processed and analyzed using the Matlab ©software environment.

The time interval counter (TIC) measurement method is shown in Figure 4.9. It divides the two sources being compared down to a lower frequency (typically 1 pulse per second) and measures their time difference with a high resolution time interval counter. In this case the reference source being the UTC (SP) and the source under test the GPS 1PPS output. The recorded information consists of 23 hours of measurements with 1 second sampling. The measured time difference, the phase data, was used then to obtain frequency data by means of a simple derivation, this is shown in Figure 4.10.

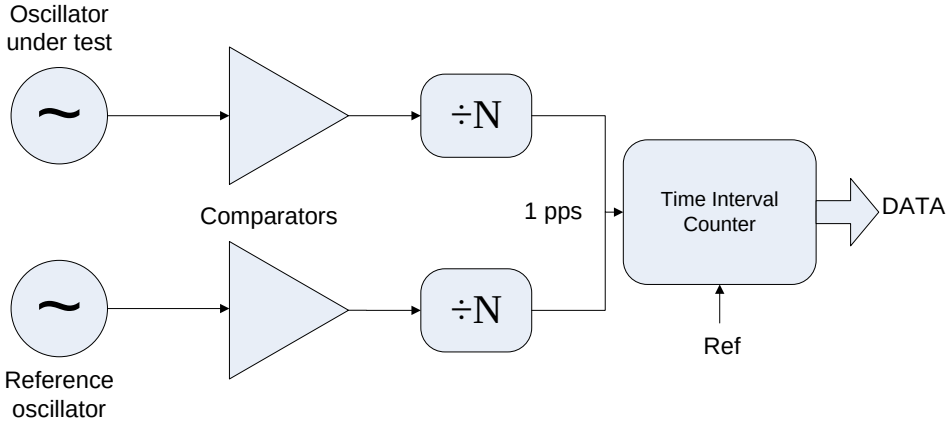

Figure 4.9: Time Interval Counter block diagram

The analysis of the frequency stability of the oscillator starts with the classification of two important factors involved in the stability as explained in section 2.5: the non-random fluctuations and the random fluctuations.

In order to determine which type of fluctuation is affecting the phase difference, a signal noise analysis was performed. An Allan deviation algorithm was implemented as explained in section 2.5.5. This algorithm was implemented on the phase data. The results are shown on Figure 4.11.

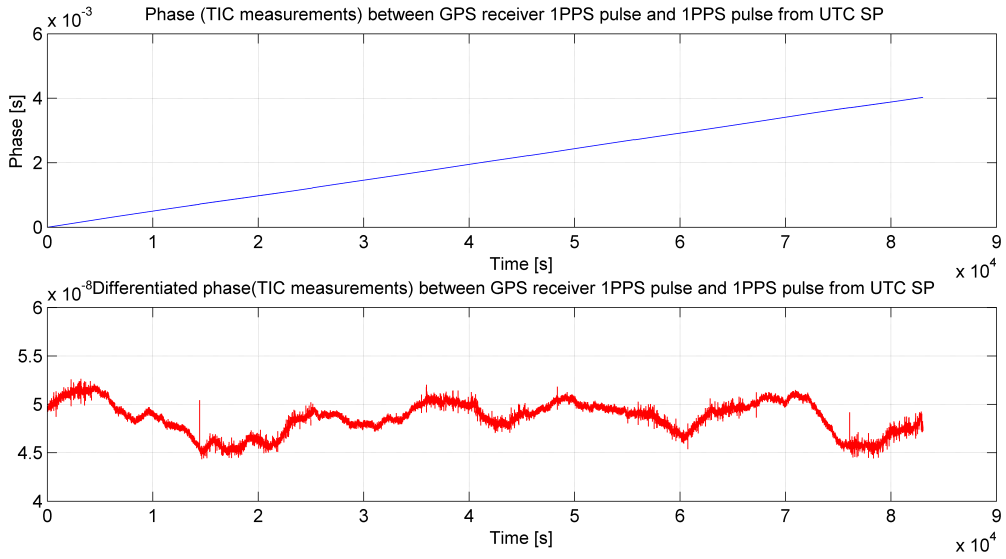

Figure 4.10: Phase and Frequency measurements from the TIC

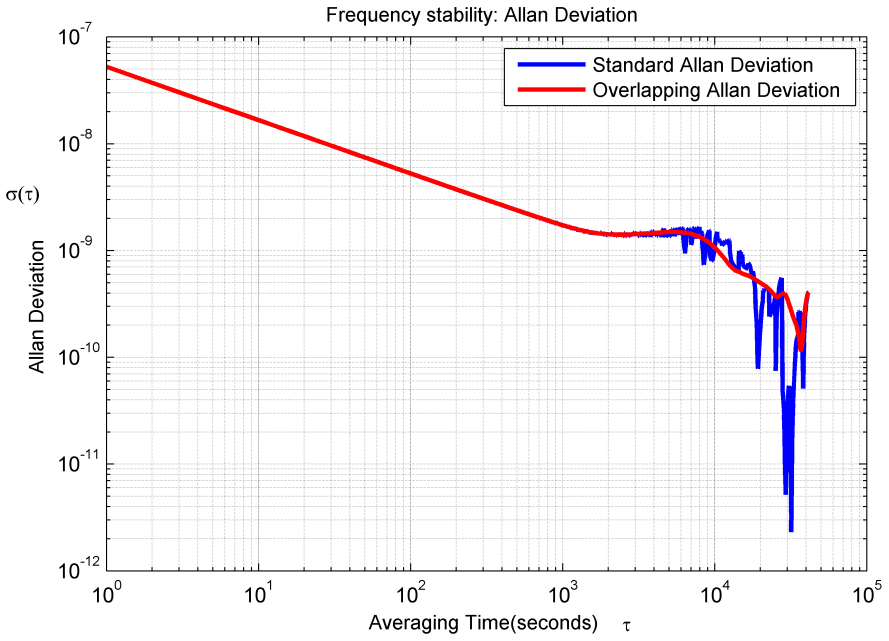

Figure 4.11: Phase and Frequency measurements from the TIC

Observing Figure 4.11 and comparing it with the sigma tau plot derived from the power-law noise one can infer that the main type of fluctuation affecting the measurements is white frequency modulation noise (White FM) due to the slope of the allan deviation results. Therefore, the next step is to analyze the derived data fron the phase difference in order to measure the standard deviation of the white noise and add it to the error budget. The standard deviation can be quantified then as:

$$\sigma_{WFnoise} = 1.63545 \times 10^{-9} \tag{4.1}$$

Having in mind the frequency of L1, 1575.42 MHz, one can compute the relative frequency error that must be also added to the error budget:

$$\sigma_{WF-L1} = 2.58 \text{ Hz} \tag{4.2}$$

4.4 Satellite Clock

A literature study as well as discussion with time and frequency experts at SP Technical Institute of Sweden shows that the relative error from the on-board satellite clocks can be quantified up to 1×10^{-11}. Considering this relative error and the GPS signal carrier frequency L1 of 1575.42 MHz one can compute the error that shall be added to the error budget:

$$\sigma_{SAT-L1} = \pm 0.0157542 \text{ Hz} \tag{4.3}$$

4.5 Atmospheric Effects

The signal propagation problems due to the properties of the ionosphere and the troposphere were studied and discussed.

When dealing with the troposhpere, the water vapour dominates the trophosperic propagation variability on shorter temporal scales. Numbers for this variability are presented in for example (Jarlemark et al., 1998). A rough calculation gives an expected Doppler shift on the order of $\approx 10^{-4}$ Hz on time scales around 1 minute.

On the other hand, dealing with the ionosphere: relatively rapid changes of the signal phase when propagating through the ionosphere is referred to as scintillations. A phase change of 1 rad could be considered as the consequence of a strong scintillation (Fu et al., 1999). On time scales around 1 minute this effect can be experienced as a Doppler shift on the order of 10^{-2} to 10^{-3} Hz. This can be believed to be the dominating unpredictable contribution from the ionosphere. The slowly varying daily phenomena is largely described by the Klobuchar model included in the broadcast message.

Considering then the worst case errors, the atmospheric errors that shall be added to the error budget are given by:

$$\sigma_{IONOSPHERE} = \approx 10^{-2} \text{ Hz} \tag{4.4}$$

$$\sigma_{TROPOSPHERE} = \approx 10^{-4} \text{ Hz} \tag{4.5}$$

These errors must be added to the error budget.

4.6 Error Budget

So far, all the errors aroused from the satellite and receiver dynamics, clocks and atmospheric effects have been analyzed and quantified. This section will then present a summarized table of all the errors in order to make up an error budget.

It is important to mention that these errors are the inherent and unmodeled errors due to the implementation of the proposed open loop approach and Doppler algorithm.

Table 4.2 shows the summarized error budget.

Error Budget(Hz)		
Error Source	**Reason/Cause**	**Magnitude(Hz)**
Satellite Dynamics	Taylors Expansion Method	± 0.0052515
Satellite clock	Rubidium/cesium clocks	$\approx \pm 0.0157542$
Receiver Dynamics	IMU time dependant errors at 51 seconds	East Component: ± 0.59235 North Component: ± 3.60957 Vertical Component: ± 0.94354
Receiver Clock	White FM Noise	± 2.58
Atmospheric Errors	Ionosphere Troposphere	$\approx \pm 10^{-2}$ $\approx \pm 10^{-4}$

Table 4.2: Error Budget

Several remarks must be introduced regarding Table 4.2. One important concern regarding the error budget has to do with the fact that the satellite and receiver dynamic errors are quantified in different coordinate systems. While the satellite dynamic errors are computed in the ECEF coordinate system, the receiver errors are presented in the ENV coordinate system. It is important to make the remark that even though the worst case scenario includes all the errors in the relative direction, mapping depending on the direction of the host vehicle will possibly reduce the unpredicted errors.

The next section will present a simple scenario in order to analyze the benefits of this approach.

4.7 Scenario

This section intends to show a high dynamic stress scenario in order to recall the benefits from the open loop approach. The scenario consists on a vehicle entering a tunnel at a velocity of 100 km/hr. After sudden breaking, the velocity at the end of the tunnel decreases down to 28 km/hr. Another important point is that at the entrance of the tunnel the open loop approach is 'switched on'.

To demonstrate the benefits of this method, an error budget is computed exactly at the end of the tunnel to compare the typical approach and the approach proposed in this thesis work.

The scenario is depicted in Figure 4.12.

This simple scenario takes into account the worst case situation. Therefore, the largest errors are summed up into the error budget without the use of any mapping. In a real situation the mapping depending on the direction of the vehicle will play an important role since the errors could be reduced.

Figure 4.13 shows the comparison between the typical and the open loop approaches. Analyzing this last Figure, one can notice that both approaches deal almost with the same errors causing a Doppler shift in the received signal. The satellite velocity calculation error

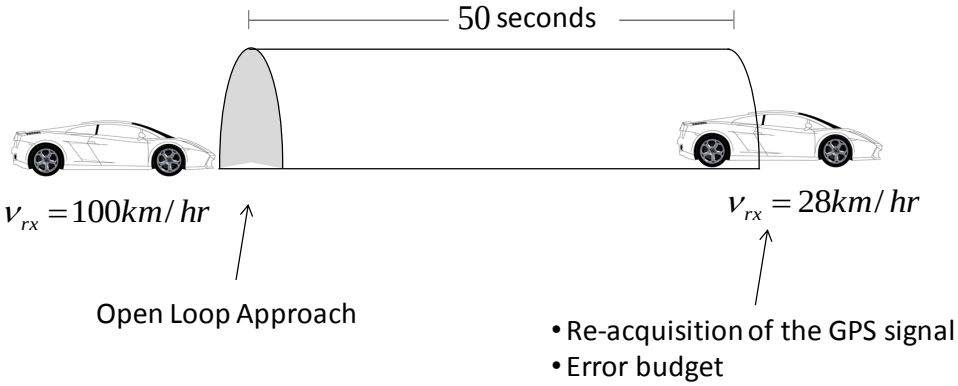

Figure 4.12: Scenario

was included in both approaches; this is due to the fact that even in a typical approach the necessary information to make this calculation is already present.

		Typical Approach	IMU Corrected
Error Source	**Reason/Cause**	**Doppler residuals (Hz)**	**Doppler residuals (Hz)**
Satellite Dynamics	Taylors Expansion Method	0.0053	0.0053
	Satellite's clock	0.0158	0.0158
Receiver Dynamics	Worst case IMU time dependant errors at 50 seconds	100	3.6096
Oscillator Dynamics	White FM Noise	2.58	2.58
Atmosphere	Troposphere	~0.0001	~0.0001
	Ionosphere	~0.001	~0.001
	TOTAL	**102.6111**	**6.2206**

Figure 4.13: Error budget

The difference in velocity of 72 km/hr at the entrance and at the end of the tunnel will inherently cause a Doppler shift of 100 Hz. This can be seen in Figure 4.13. However with the open loop approach this Doppler shift is reduced considerably down to around 6 Hz. Another perspective to show the improvement is by analyzing the block diagrams depicting both approaches, shown in Figure 4.14 and 4.15.

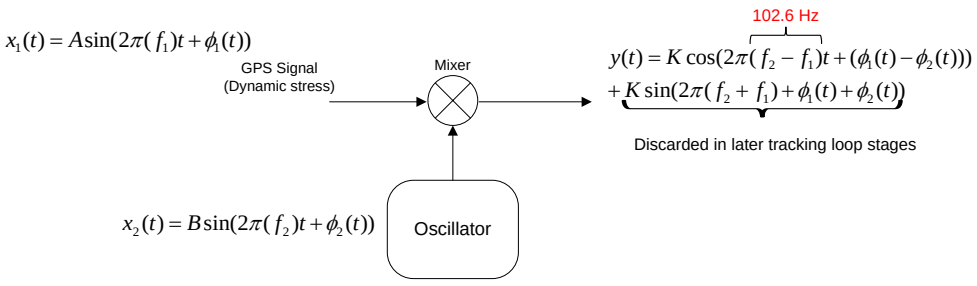

Figure 4.14: Block diagram for a typical approach

Figures 4.14 and 4.15 show the block diagram of the initial stage in the tracking loop. The typical approach consists of the oscillator, while the open loop approach includes the Doppler model that will drive the oscillators' frequency to match the frequency from the received signal. This last perspective shows how the next stages of the GPS receiver will deal specifically with an almost "dynamic free" signal. This improvement will reduce the

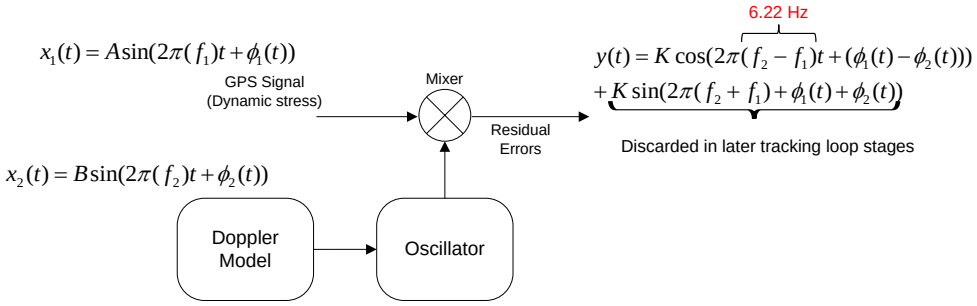

Figure 4.15: Block diagram for an open loop approach

need of a high bandwidth in the loop filter to track the signal; less bandwidth induces improved signal to noise ratio.

The Doppler correction will also allow the receiver to track the signals faster. This improvement merely allows performing a faster re-acquisition of the signal due to temporary blockage or weak signal environment conditions.

5 Discussion and Conclusion

5.1 Discussion

This thesis work has presented an open approach tracking approach using ultra-tight GPS/IMU strategies. A methodology has been proposed to deal with the satellite, receiver and oscillator dynamics. From the methodology, an error budget was calculated given specific acceleration and oscillator measurements. A scenario was presented in order to show the importance of the dynamics removal and its relationship with the loop bandwidth of the PLL and the signal to noise ratio of the system. However, several important points need to be discussed.

The available accelerometer measurements obtained from IMEGO IMT40 have several issues that must be taken into account. The measurements were performed without any specialized alignment measuring and little information about the gyroscopes and direction correction algorithms. Furthermore, IMEGO's INS was mounted on an industrial mechanical arm robot where inherent vibrations and stabilization issues may be involved and possibly becoming an hypothesis for the error difference in the north component compared to the east and north ones.

The presented scenario does not involve any possible errors regarding the behavior of the inertial sensors when dealing with high dynamics. It is expected that the sensitivity of the sensors will vary depending on the dynamics applied to them. The latter issue is suggested as a study to see how the sensors react to different acceleration scenarios.

The theory proposed in the open loop approach shows to be a benefitial solution for the improvement in the signal to noise ratio by reducing significantly the bandwidth in the PLL and thus in the system in general making it possible to implement in low. However, due to the previously discussed issues the next research step shall consider focusing efforts to test the system performance as a whole, involving GPS data and INS data in a higher dynamics scenario such as an automobile. Further work shall involve reducing the error budget. An analysis on the error budget components shall be made in order to decide which number can be further reduced to improve the approach. This can involve the use of high quality oscillators, inertial sensors, the use of more complex signal processing to improve the navigation solution.

Finally, new GNSS systems can be taken into account. The satellite dynamics will differ

from system to system. However, different data and signals can be used to take advantage of their properties and eventually improve the satellites dynamic estimation.

5.2 Conclusion

The proposed methodology and Doppler model provides a solution for the weak signal environments where higher signal noise to ratio is required. The proposed Doppler model provides an algorithm to account for the satellite dynamics with an accuracy of $\pm.0005$ Hz for the Doppler error. A literature study was performed to quantify the Doppler errors due to the satellite clock as well as the atmospheric effects. It is shown that the errors from the IMU are dominant in the error budget. The errors introduced by the receiver oscillator are also shown to be significant with up to 2.58 Hz for L1 GPS signal. For a scenario where a vehicle enters a tunnel at 100 km/h and 50 seconds later exits the tunnel with a speed of 28 km/h it is shown that the dynamics of the signal can be reduced from 100 Hz to 6 Hz after implementing the open loop approach.

The implementation of the Doppler model shows to be less complex than actual closed loop navigation architectures and keeps the same main benefits intact. This thesis work provides a base for future indoor research navigation since a lot of factors have to be still accounted.

References

Babu, R. and Wang, J. (2005). Analysis of ins derived doppler effects on carrier tracking loop. *The Journal of Navigation*, 58:493–507.

Brown, R. and Hwang, P. (1997). *Introduction to Random Signals and Applied kalman Filtering*. John Wiley and Sons, United States.

Chiou, T.-Y. (2005). Gps receiver performance using inertial-aided carrier tracking loop. Technical report, Stanford University. Presented at the Institute of Navigation GNSS Conference.

Farrel, J. and Barth, M. (1999). *The Global Positioning System and Inertial Navigation*. McGraw-Hill, New York, USA.

Fu, W., Shaowei, H., Rizos, C., Knight, M., and Finn, A. (1999). Real-time ionospheric scintillation monitoring. *ION GPS 99*.

Gebre-Egziabher (2007). What is the difference between 'loose', 'tight', 'ultra-tight' and 'deep' integration strategies for ins and gnss? *GNSS Solutions*, January/February:28–33.

Grewal, M. e. a. (2001). *Global Positioning Systems, Inertial Navigation, and Integration*. John Wiley and Sons, New York, USA.

Grewal, M. e. a. (2007). *Global Positioning Systems, Inertial Navigation, and Integration*. John Wiley and Sons, New Jersey, USA, second edition.

Hofmann-Wellenhoff, B. (2001). *GPS: Theory and Practice*. Springer-Verlag Wien, New York, USA.

Jarlemark, P., Emardson, T., and Johansson, J. (1998). Wet delay variability calculated from radiometric measurements and its role in space geodetic parameter estimation. *Radio Science*, 33:719–730.

Kaplan, E. (2006). *Understanding GPS: principles and applications.* Artech House, USA.

Kleeman, L. (1996). Proceedings of the seecond workshop on perceptive systems. In *Understanding and Applying Kalman Filtering.*

Leick, A. (1990). *GPS Satellite Surveying.* John Wiley and Sons, USA.

Marshall, J. (2002). Gps toolbox: Creating and viewing skyplots. *GPS Solutions*, 6:118–120.

Remondi, B. (2004). Computing satellite velocity using the broadcast ephemeris. *GPS Solutions*, 8:181–183.

Riley, W. (2008). Handbook of frequency stability analysis. Technical report, National Institute of Standards and Technology.

Titterton, D. (2004). *Strapdown Inertial Navigation Technology.* The Institution of Electrical Engineers and The American Institute of Aeronautics and Astronautics, United Kingdom.

USCGNV (1993). Interface control document. Technical report, U.S. Coast Guard Navigation Center.

Welch, G. (2006). An introduction to the kalman filter. Technical report, University of North Carolina of Chapel Hill.

Woodman, O. (2007). An introduction to inertial navigation. Technical report, University of Cambridge.

Zhang, J. (2006). Gps satellite velocity and acceleration determination using the broadcast ephemeris. *The Journal of Navigation*, 59:293–305.

Zhang, W. (2009). Proceedings of the european navigation conference - global navigation satellite systems. In *Extension of GPS Broadcast Ephemeris to Determine Satellite Velocity and Acceleration.*